DEEP LEVELS AND HIGH CONCENTRATIONS OF IMPURITIES IN SILICON

Thesis by

Tsu-wei Frank Lee

In Partial Fulfillment of the Requirements

for the Degree of

Doctor of Philosophy

California Institute of Technology

Pasadena, California 91109

(Submitted August , 1974)

To my parents

ACKNOWLEDGMENTS

All my grateful thanks go to Dr. James W. Mayer and Dr. Thomas C. McGill for their constant guidance and encouragement throughout the course of this work. I would like to acknowledge Dr. Marc-A. Nicolet for exciting discussions. Assistance by Rob Gorris was helpful. Mrs. Kathleen Ellison and Mrs. Carol Norris did all the typing. To them go my sincere thanks.

ABSTRACT

(1)

A study of the electronic levels associated with the divacancy in silicon is reported. The extended Hückel theory is shown to reproduce the band structure near the energy gap of silicon. The electronic levels of the divacancy are calculated by considering a periodic array of large unit cells each containing 62 atoms; a 64 atom perfect cell with 2 atoms removed to form the divacancy. The results are found to be in qualitative agreement with the results of EPR and infrared absorption measurements.

(2)

A theory of the variation of conduction electron density with the temperature for various impurity concentrations is presented. In addition to previously noted effects of conduction band edge lowering and screening of the impurity potential by the conduction electrons, the influence of a finite energy transfer integral and spatial fluctuation in the potential are included. The results show that for $N_D \lesssim 10^{17}$ cm^{-3} in silicon one must not view the activation as occurring between a single impurity level and a well defined conduction band edge, but must include the broadening of the impurity level and tailing of the conduction band density of states. Calculations for the shallow donors P, Sb, and As in Si are found to be in satisfactory agreement with experiment.

(3)

Hall and sheet resistivity measurements as a function of temperature combined with layer removal have been used to study Si implanted with Te at energies up to 220 KeV. At low doses ($\lesssim 4 \times 10^{12}$ cm^{-2}), Te has a donor level with 140 meV activation energy. The activation energy decreases at higher Te doses and is approximately equal to zero for Te doses $\gtrsim 10^{15}$ cm^{-2}. At high dose levels, the number N_s of conduction electrons is more than an order of magnitude below the number of Te cm^{-2}. High temperature anneal treatments followed by quenching did not produce a substantial increase in N_s suggesting that the formation of Te clusters was not responsible for the low value of N_s. Also channeling measurements indicated a high substitutional fraction. Based on differential Hall measurements on P-implanted samples, with and without Si pre-damage, we conclude that residual radiation damage is not a major factor. A theoretical calculation, which includes the effect of decrease of activation energy with increasing impurity concentrations, indicated that the number of conduction electrons could be much less than the number of implanted Te even though the apparent activation energy is almost zero. Although the results of theoretical calculation do not give quantitative agreement with the experimental results, they do confirm the changes in apparent activation energy with concentration.

TABLE OF CONTENTS

PART ONE

INTRODUCTION

Deep level impurities in semiconductors[1] are of considerable interest because they have been found to create important effects in the devices. For examples, the presence of gold in silicon junction can increase the switching speed;[2] the deep level features of nitrogen impurities are responsible for the high quantum efficiency of gallium phosphide light emitting diode.[3] Also, there has been a upsurge of interest in heavily doped semiconductors.[4] This interest is both due to their expanding applications and their new phenomena in the semiconductor physics. This thesis contains both theoretical and experimental studies addressed to the problem of deep levels and high impurity concentrations in silicon.

Deep levels in semiconductors have been the subject of study for about 20 years. Until recently, very little theoretical work has been reported on this difficult problem. The theoretical complication is due to the tight binding character and multiplicity of charge states which are usually associated with deep levels. In addition, the lattice distortion around the defect center has also been thought to have significant influence on the deep energy levels. Therefore, the effective mass theory, which works successfully for shallow levels, is not applicable to deep level problems. An appropriate theory for deep levels should correctly take into account the defect center potential, electron-electron interaction and the lattice distortions, simultaneously.

There have been two different kinds of approaches to treat the deep level problems. One is the solid state scattering theory

(SST) used by Callaway[5] and the other is the defect molecular model (DMM) pioneered by Coulson and Kearsley.[6] In the SST, the solid state continuum aspects of the problem are emphasized. The defect energy level is calculated in terms of scattering of electrons off the defect center potential. The tremendous amount of work in this calculation makes it difficult to incorporate the electron-electron interaction and lattice distortions into the solid state scatering theory. The SST has been applied to undistorted vacancy[7] and undistorted divacancy[8] in silicon. The lattice distortions were neglected in their calculations.

In the defect molecular model, one considers all the bonds near the defect center and treats them like a molecular unit. A full configuration interaction, electron-electron interaction and Jahn-Teller distortion are included in this model. This model has been applied with moderate success to vacancy[6,9,10] and divacancy[11] in diamond. Because of the complicated calculations involved, it is difficult to extend this model to a molecular unit with a large number of atoms. Hence, the influence of the bonds other than the nearest ones are not included. This makes this method not suitable for defect centers of which the amplitude of the electron wavefunction extends over more than just the nearest bonds. Furthermore, since the solid state continuum aspect is totally lost in this molecular model, the relative position of the defect levels with respect to the solid state band diagram can not be determined.

Recently, Messmer and Watkins[12] have modified the DMM so

that they can treat large molecular unit. In the modified DMM, they have used the extended Huckel theory (EHT),[13] ~~which is a one-~~ which is a one-electron molecular-orbital treatment, on a finite cluster of atoms to investigate the nature of deep defect levels. Lattice distortions are directly included by moving atoms in the cluster about until the total energy of the system reached a minimum. However, the variation of electron-electron interaction and ion-ion interaction with charge state and distortion were not included in this treatment. It has also been pointed out that, by directly applying the EHT to cluster of atoms, the energy levels and the ordering of the symmetry depend upon the size of the cluster selected.[14,15]

In Part II of this thesis, we have used the EHT to calculate deep energy levels. Due to the inherent complication of deep level problems, we chose a simple system to study: divacancy in silicon. It has been suggested[16] that divacancy in silicon introduces three levels in the energy gap, with four charge states (+1, 0, -1 and -2); the single donor state is located approximately at 0.25 eV above the valence band edge and the double acceptor state is at about 0.4 eV below the conduction band edge. Watkins and Corbett[16] deduced a model for lattice distortion around the silicon divacancy by using their electron-paramagnetic-resonance data. Furthermore, suggested by the results of EPR and stress experiments, Watkins[17] claimed that the energy associated with this lattice distortion was about 2 eV and thus had significant influence on the energy levels. We have used the model of Watkins and Corbett to include the distortion around the silicon divacancy. That is, we applied

the EHT to a system of periodic large unit cell with a distorted divacancy in each cell. This treatment differs from that of Messmer and Watkins in that they used a cluster of atoms to calculate energy level of nitrogen in silicon whereas we used a solid which consisted of periodic large unit cell.

As to heavily doped semiconductors, it has been reported that the impurity-to-band activation energy decreases with increasing impurity concentrations.[18] A number of different suggestions have been put forward to account for this phenomenon theoretically. Pearson and Bardeen,[18] and Castellan and Seitz[19] suggested that the decrease of impurity activation energy with impurity concentrations was due to attraction between the conduction electrons and ionized donors. Calculations based upon this physical model yielded qualitative but not quantitative agreement with the experimental results. Pincherle[20] proposed that free carriers screen the field of the impurity center and hence give rise to decrease of electron binding energy to the impurity center. Calculations based upon this proposal only did not give satisfactory results. A self-consistent calculation which combined the above two models was given by Lehman and James.[21] Their calculation gave a better agreement with experimental results but still underestimated the decrease of activation energy.

It should be pointed out that both the shift of impurity level with respect to band edge and the broadening of impurity level could lead to variation of impurity activation energy. The impurity level shift may be due to the above mentioned physical phenomena,

i.e. conduction electron screening and Coulombic attraction. The impurity level broadening may be caused either by the finite energy transfer integral due to wavefunction overlap or by potential fluctuations. In the first case, the impurity level wavefunction at a given impurity has finite Hamiltonian matrix elements with impurity level wavefunction centered at nearby impurities. This leads to finite energy transfer integral and to broadening of impurity levels when the impurities are at finite density. This produces a band of levels. In the second case, the presence of charged impurities distributed in a random way throughout the solid generated potential fluctuations. These potential fluctuations produce tailing of conduction and valence band density-of-states[22] and spreading of impurity levels.[23] In Part III of this thesis, we will include both the shift and the broadening of the impurity level to treat the decrease of impurity activation energy with impurity concentrations.

Generally, deep level impurities have low solid solubility in semiconductors and thus it is difficult to heavily dope the semiconductors with deep level impurities by thermal equilibrium techniques. However, ion implantation provides a way to introduce high concentrations of deep level impurities, even above their solid solubilities, in semiconductors. After ion implantation, usually high temperature anneal (600-850 $^{\circ}$C) is required to reduce the radiation damage in the ion implanted samples. Therefore, even though ion implantation can introduce impurities above their solid solubility into semiconductors, after high temperature anneal, the impu-

rities may precipitate by forming compounds or moving out of lattice sites and become electrically inactive. Channeling measurement provides a tool for studying the impurity lattice location.[24] MeV He ion backscattering and channeling measurements have been made for lattice locations of group II and group VI elements in silicon.[25] Of these elements, tellurium is attractive because it has large fraction (60%) on substitutional sites.[24]

Tellurium has been reported to be a donor in silicon. ~~and~~ For Te concentration less than 10^{17} cm^{-3}, ~~and~~ it has a deep level, 0.14 eV, below the conduction band edge.[26] Previous Hall effect and resistivity measurements[27] indicated that for heavily Te implanted samples the number of conduction electrons/cm^2 is much lower than that of implanted substitutional Te/cm^2 even though the activation energy is almost zero. The discrepancy in these numbers may be due to the fact that the measured number of conduction electrons/cm^2 is a weighted average of the implanted impurity concentrations and is usually smaller than the number of implanted impurities. Another source for this discrepancy is that high temperature anneal after ion implantation may still leave some residual damage. The residual damage may act like a compensation centers and thus reduces the number of conduction electrons/cm^2. In arsenic diffused samples, it has been found[28] that the electrical activity is reduced by long heat treatment at temperatures of 500-970 °C. The electrical activity could be increased by heating at high temperatures (~1100 °C) and then quenching. The reduction of electrical activity was attributed to the formation of As clusters which could be dissociated during

high temperature processing. Similar effects may be responsible for this discrepancy in high dose Te implanted samples.

In Part IV of this thesis, we performed Hall effect and resistivity measurements combined with layer removal technique to investigate the electrical properties of Te implanted silicon samples. Theoretical calculations of conduction electrons/cm^3 as a function of temperature for Te in silicon were also made. The calculated results were then compared with experimental data.

REFERENCES

1. A.G. Milnes, Deep Level Impurities in Semiconductors, Wiley-Interscience, New York (1973).
2. W.M. Bullis, Solid State Elec. 9, 143 (1966).
3. C.B. Duke and N. Holonyak Jr., Phys. Today, December (1973).
4. V.I. Fistul, Heavily Doped Semiconductors, Plenum Press, New York (1969).
5. J. Callaway, J. Math. Phys. 5, 783 (1964).
6. C.A. Coulson and N.J. Kearsley, Proc. Roy. Soc. A241, 433 (1957).
7. J. Callaway and A.J. Hughes, Phys. Rev. 156, 860 (1967).
8. J. Callaway and A.J. Hughes, Phys. Rev. 164, 1043 (1967).
9. C.A. Coulson and F.P. Larkins, J. Phys. Chem. Solids 32, 2245 (1971).
10. F.P. Larkins, J. Phys. Chem. Solids 32, 2123 (1971).
11. C.A. Coulson and F.P. Larkins, J. Phys. Chem. Solids 30, 1963 (1969).
12. R.P. Messmer and G.D. Watkins, Phys. Rev. Lett. 25, 656 (1970).
13. R. Hoffman, J. Chem. Pgys. 39 1397 (1963).
14. F.P. Larkins, J. Phys. Chem. Solids 4, 3065 (1971).
15. F.P. Larkins, J. Phys. Chem. Solids 4, 3077 (1971).
16. G.D. Watkins and J.W. Corbett, Phys. Rev. 138, A543 (1965).
17. G.D. Watkins, Radiation Efeects in Semiconductors, (ed. by F.L. Vook, Plenum, New York, 1968) P. 67.
18. G.L. Pearson and J. Bardeen, Phys. Rev. 75, 865 (1949).
19. G.W. Castellan and F. Seitz, Semiconducting Materials, (Butterworths, London, 1951) P. 8.

20. L. Pincherle, Proc. Phys. Soc. (London) A64 663 (1951).

21. G.W. Lehman and H.M. James, Phys. Rev. 100, 1698 (1955).

22. E.O. Kane, Phys. Rev. 131 79 (1963).

23. T.N. Morgan, Phys. Rev. 139, A343 (1965).

24. S.T. Picraus, N.G.E. Johansson and J.W. Mayer, Semiconductor Silicon, Electrochem. Soc., Inc., New York, 422 (1969).

25. J. Gyulai, O. Meyer, R.D. Pashley and J.W. Mayer, Rad. Effects 7, 17 (1971).

26. S. Fischler, Metallurgy of Advanced Electronic Materials, Interscience 19, New York (1963).

27. N.G.E. Johansson, J.W. Mayer and O.J. Marsh, Solid State Elec. 13, 317 (1970).

28. R.O. Schwenker, E.S. Pan and R.F. Lever, J. Appl. Phys. 42, 3195 (1971).

PART TWO

SEMI-EMPIRICAL CALCULATION OF DEEP LEVELS: DIVACANCY IN SILICON

1. INTRODUCTION

Up until recently, very little theoretical work has been reported on the difficult questions associated with deep levels in semiconductors. This lack of theoretical activity is not due to a lack of experimental information on deep levels but is due to the inherent theoretical complications thought to be associated with the deep level problem. The tightly bound character and multiplicity of charge states usually associated with deep levels make the standard effective mass theory (Kohn 1957) inappropriate. An appropriate theory of the deep electronic levels is thought to require the simultaneous accurate treatment of the potential of the defect, the lattice distortion, and the electron-electron interaction.

Previous theoretical treatments of defect levels have made use of two rather different approaches. The first pioneered by Coulson and Kearsley (1957) and extended by Coulson and Larkins (1969 and 1971) makes use of the defect molecule model (DMM). In the DMM, one approximates the problem of a defect in a perfect solid by a small molecular unit consisting of the bonds near the defect. A full configuration interaction calculation is then performed on this small molecular unit. Lattice distortion is treated by expanding the energy of the defect molecule to second order in the atomic positions and minimizing this expansion to obtain the atomic positions and energy eigenvalues. While the DMM takes account of electron-electron interaction explicitly, the difficult calculations inherent in the method have prevented calculations

involving more than the bonds on the nearest neighbors. Hence, the influence of bonds further away from the defect have not been included. This makes the method unsuitable for the treatment of defects where the amplitude of the wavefunction of an electronic level associated with the defect extends over more than just the nearest bonds. The DMM has been applied with moderate success to the vacancy in diamond by Coulson and Kearsley (1957), Coulson and Larkins (1971), and Larkins (1971a) and to the divacancy in diamond by Coulson and Larkins (1969).

Recently, Messmer and Watkins (1970) have modified the DMM so that one can treat larger molecular units. In their calculations, a finite cluster of atoms is treated using the extended Hückel theory (EHT) (Hoffman 1963). Lattice distortions are treated directly by moving atoms in the cluster about until the total energy of the system reaches a minimum. The application of the EHT to the cluster, on the one hand, makes it possible to treat very large clusters of atoms. However, on the other hand, it does not take account explicitly of the variation of electron-electron interaction and ion-ion interaction with charge state and distortion (Larkins 1971 b,c).

Messmer and Watkins (1971) and Watkins and Messmer (1970) have applied these techniques with moderate success to a number of deep levels in diamond. However, Larkins (1971 b,c) has shown that direct application of these methods to defects in silicon presents a number of problems. The energy gap between occupied and unoccupied levels is much larger than the band gap. The energy eigenvalues and the

ordering of eigenvalues of various symmetry depend upon the size of the cluster selected.

The second approach makes use of solid state scattering theory (SST) (Callaway 1964). In this approach, the solid state continum aspects of the problem are emphasized. The defect level problem is cast in terms of the scattering of an electron off the defect potential in the presence of a perfect crystal (Bennemann 1965; Callaway and Hughes 1967). However, the method has the disadvantages that: it is difficult to identify the correct form of the defect potential; the treatment of lattice distortion and electron-electron interaction is hard to carry out; and a great deal of calculational work is required to obtain results.

In this paper, we report upon a study of a deep level in silicon, the divacancy. In this study, we have attempted to marry some of the best points of the two methods described above. To do this, we have made calculations using the EHT for a perfect solid consisting of large unit cells with the divacancies at their center. Hence, we have a well defined potential (the absence of two silicon atoms) and at the same time we have circumvented the difficulties associated with cluster calculations which have been noted above. Using this method, we obtain results which are in qualitative agreement with known experimental results.

The outline of this paper is as follows: In Section 2, we review the theoretical approach. In Section 3, we report the results obtained for the silicon divacancy. Section 4 contains discussions and conclusions.

2. OUTLINE OF THEORY

2.1 Extended Hückel Theory (EHT)

In the independent electron approximation, the energy eigenvalues and eigenfunctions for a system consisting of a defect in an otherwise perfect solid are obtained by solving the time independent Schrodinger equation,

$$H\psi_i = \varepsilon_i\psi_i \quad , \qquad (2.1)$$

where ,

$$H = H_{perfect} + V_{defect} \quad . \qquad (2.2)$$

V_{defect} is defined to be the difference in potential between that found in a perfect crystal and that found with the defect present. One approach to solving (2.1) is to take ψ_i to be a linear combination of atomic orbitals, ϕ_α, centered on each atom in the crystal. That is,

$$\psi_i = \sum_\alpha C_{i\alpha}\phi_\alpha \quad . \qquad (2.3)$$

In this case, a solution to (2.1) is obtained when

$$\det|H_{\alpha\beta} - \varepsilon S_{\alpha\beta}| = 0 \quad , \qquad (2.4)$$

where

$$H_{\alpha\beta} = \langle\phi_\alpha|H|\phi_\beta\rangle \quad , \qquad (2.5)$$

and

$$S_{\alpha\beta} = \langle \phi_\alpha | \phi_\beta \rangle \quad . \quad (2.6)$$

In the EHT, the matrix elements of the Hamiltonian between the atomic orbitals is approximated by taking

$$H_{\alpha\beta} = -\frac{1}{2} K_{\alpha\beta}(I_\alpha + I_\beta)S_{\alpha\beta} \text{ , for } \alpha \neq \beta \quad ; \quad (2.7a)$$

and

$$H_{\alpha\alpha} = - I_\alpha \quad . \quad (2.7b)$$

I_α is the empirical ionization energy of the αth atomic level and $K_{\alpha\beta}$ is a dimensionless parameter usually taken to be between 1 and 2.

2.2 Large Unit Cell

The method of Messmer and Watkins (1970) consists of the application of (2.4) to (2.7) to a large cluster of atoms with the defect in the center. However, as will be discussed below, direct application of this method leads to unsatisfactory results.

To solve this problem, we have considered a perfect solid with a large unit cell. The large unit cell was chosen to consist of a cubic block of two by two by two face centered cubic cells, 32 primitive cells, or 64 atoms. This procedure insures that a calculation for a system with no defects will give an exact energy gap.

2.3 Lattice Distortion

The position of the atoms near the defect should be obtained by minimizing the total energy of the system with respect to atomic positions. The quantity in the EHT which is analogous to the total energy of the

system is defined as

$$E_{EHT} = \sum_i \epsilon_i \quad , \qquad (2.8)$$

where the summation runs over all the occupied states. Messmer and Watkins (1970) have used this expression for the energy to obtain the lattice distortion of the atoms in a cluster about the defect. The same process could be used with a little bit more work to calculate the lattice distortion in a large unit cell as discussed above. However, as emphasized by Larkins (1971 b,c), the total energy defined by (2.8) is not precisely the total energy of the system since no explicit provision is made for taking account of electron-electron interaction, and ion-ion interaction variation with charge state and lattice distortion. Hence, minimizing (2.8) to give the equilibrium atomic positions about the defect may give unreliable results. For this reason, we have decided to simply explore the role of lattice distortion on the electronic levels associated with the defect.

We will only report on one representative distortion here. The lattice distortion chosen is suggested by that deduced by Watkins and Corbett (1965) with the aid of their EPR data, see Fig. 1. The pairs of atoms a and c, and a' and c' are moved toward each other to improve the bonding between the "dangling bonds" left by the removal of the divacancy atoms, while the atoms b and b' are moved away from each other so that they move out of the way of the bonding pairs, ac and a'c'. Further, the distortion was introduced in such a way that the distortion of the bonds between the atoms next to the defect and their three nearest neighbors

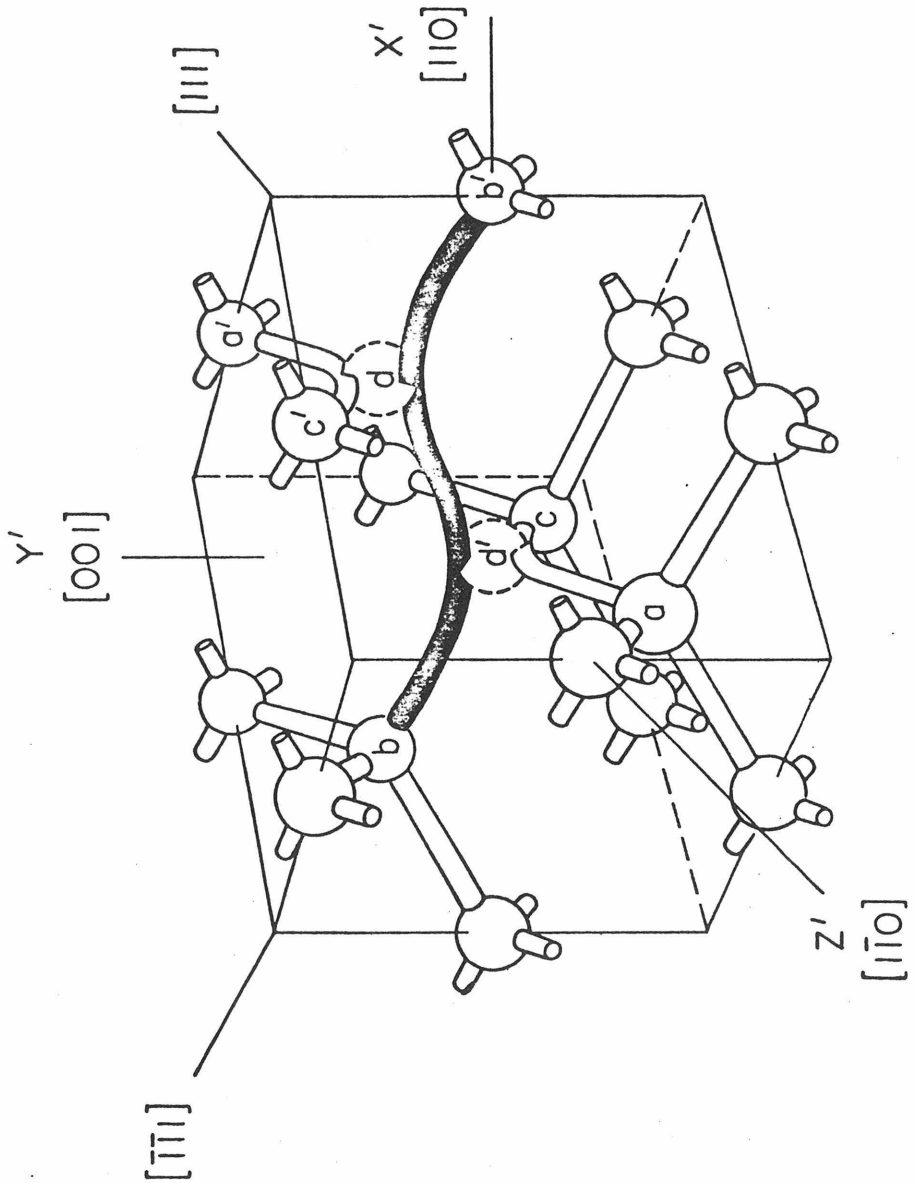

Figure 1 The model of divacancy defect in silicon deduced from EPR studies.

was confined to the stretching a single bond and the bending of the other two bonds. If we take the location of the six nearest neighbor atoms to the divacancy in the undistorted case to be given by:

$$\vec{a} = a_o(\vec{e}_x - 3\vec{e}_y - 3\vec{e}_z)/8 \quad , \quad (2.9a)$$

$$\vec{a}' = a_o(-\vec{e}_x + 3\vec{e}_y + 3\vec{e}_z)/8 \quad , \quad (2.9b)$$

$$\vec{b} = a_o(-3\vec{e}_x - 3\vec{e}_y + \vec{e}_z)/8 \quad , \quad (2.9c)$$

$$\vec{b}' = a_o(3\vec{e}_x + 3\vec{e}_y - \vec{e}_z)/8 \quad , \quad (2.9d)$$

$$\vec{c} = a_o(-3\vec{e}_x + \vec{e}_y - 3\vec{e}_z)/8 \quad , \quad (2.9e)$$

$$\vec{c}' = a_o(3\vec{e}_x - \vec{e}_y + 3\vec{e}_z)/8 \quad . \quad (2.9f)$$

where a_o is the length of the cube edge, then, after the distortion, the atoms are located at

$$\vec{a} = a_o[(1-\beta)\vec{e}_x - (3-\beta)\vec{e}_y - (3+\alpha)\vec{e}_z]/8 \quad , \quad (2.10a)$$

$$\vec{a}' = a_o[-(1-\beta)\vec{e}_x + (3-\beta)\vec{e}_y + (3+\alpha)\vec{e}_z]/8 \quad , \quad (2.10b)$$

$$\vec{b} = a_o[-(3+\beta)\vec{e}_x - (3+\beta)\vec{e}_y + (1+\alpha)\vec{e}_z]/8 \quad , \quad (2.10c)$$

$$\vec{b}' = a_o[(3+\beta)\vec{e}_x + (3+\beta)\vec{e}_y - (1+\alpha)\vec{e}_z]/8 \quad , \quad (2.10d)$$

$$\vec{c} = a_o[-(3-\beta)\vec{e}_x + (1-\beta)\vec{e}_y - (3+\alpha)\vec{e}_z]/8 \quad , \quad (2.10e)$$

$$c' = a_o[(3-\beta)\vec{e}_x - (1-\beta)\vec{e}_y + (3+\alpha)\vec{e}_z]/8 \quad . \quad (2.10f)$$

α sets the scale of the distortion and

$$\beta = \sqrt{\frac{4\alpha - \alpha^2}{2}} \quad .$$

Distortion is measured by a parameter d defined by

$$d = a_0\sqrt{\alpha}/4 \quad . \qquad (2.11)$$

2.4 Definition of Localization

For the purpose of deciding which levels should be identified with the defect, we define a measure of localization of a level i on the six nearest neighbor atoms by:

$$P_i = \frac{\sum_{\substack{\alpha,\beta \\ \text{over six atoms}}} C^*_{i\alpha} C_{i\beta} S_{\alpha\beta}}{\sum_{\substack{\alpha,\beta \\ \text{all atoms} \\ \text{unit cell}}} C^*_{i\alpha} C_{i\beta} S_{\alpha\beta}} \quad , \qquad (2.12)$$

where $C_{i\alpha}$ is the α^{th} component of eigenvector of state i.

3. RESULTS

3.1 Silicon Band Structure

For suitable values of EHT parameters in (2.7), the EHT accurately reproduces the accepted band structure for silicon (Herman et al. 1966; Messmer 1971). We have used atomic functions like those obtained by Clementi (1965). The atomic functions used differ in that we have kept only the three largest terms in the expansion in Slater orbitals and modified the Slater exponents slightly. The Slater exponents in ϕ_{3s} are increased by factor of 1.3 and the Slater exponents in ϕ_{3p} by 1.4,

$$\phi_{3s} = [- 0.20265\ \chi_3(6.8112, r) + 0.61435\ \chi_3(2.7160, r) + 0.52025\ \chi_3(1.6829, r)]\ Y_{0,0}(\theta, \phi) \quad , \quad (3.1)$$

and a 3p wave function of the form

$$\phi_{3p} = [- 0.1208\ \chi_2(9.8, r) + 0.48091\ \chi_4(3.2214, r) + 0.57523\ \chi_4(1.8218, r)]\ Y_{1,0}(\theta, \phi) \quad , \quad (3.2)$$

where

$$\chi_n(\xi, r) = [a_B{}^3(2n)!]^{-\frac{1}{2}}\ (2\xi)^{n+\frac{1}{2}}\ (\frac{r}{a_B})^{n-1}\ e^{-\xi r/a_B}$$

and a_B is Bohr radius.

$$I_{3s} = 17 \text{ eV} \quad , \quad (3.3a)$$

$$I_{3p} = 11.6 \text{ eV} \quad . \quad (3.3b)$$

The dimensionless parameters were taken to be

$$K_{ss} = 1.87 \quad , \quad (3.4a)$$

$$K_{pp} = 1.81 \quad , \quad (3.4b)$$

$$K_{sp} = 1.35 \quad (3.4c)$$

Using these parameters, we obtain the band structure shown in Fig. 2. The calculated value of the gap is 1.15 eV and the minimum in the conduction band occurs along the Δ direction in agreement with accepted band structures.

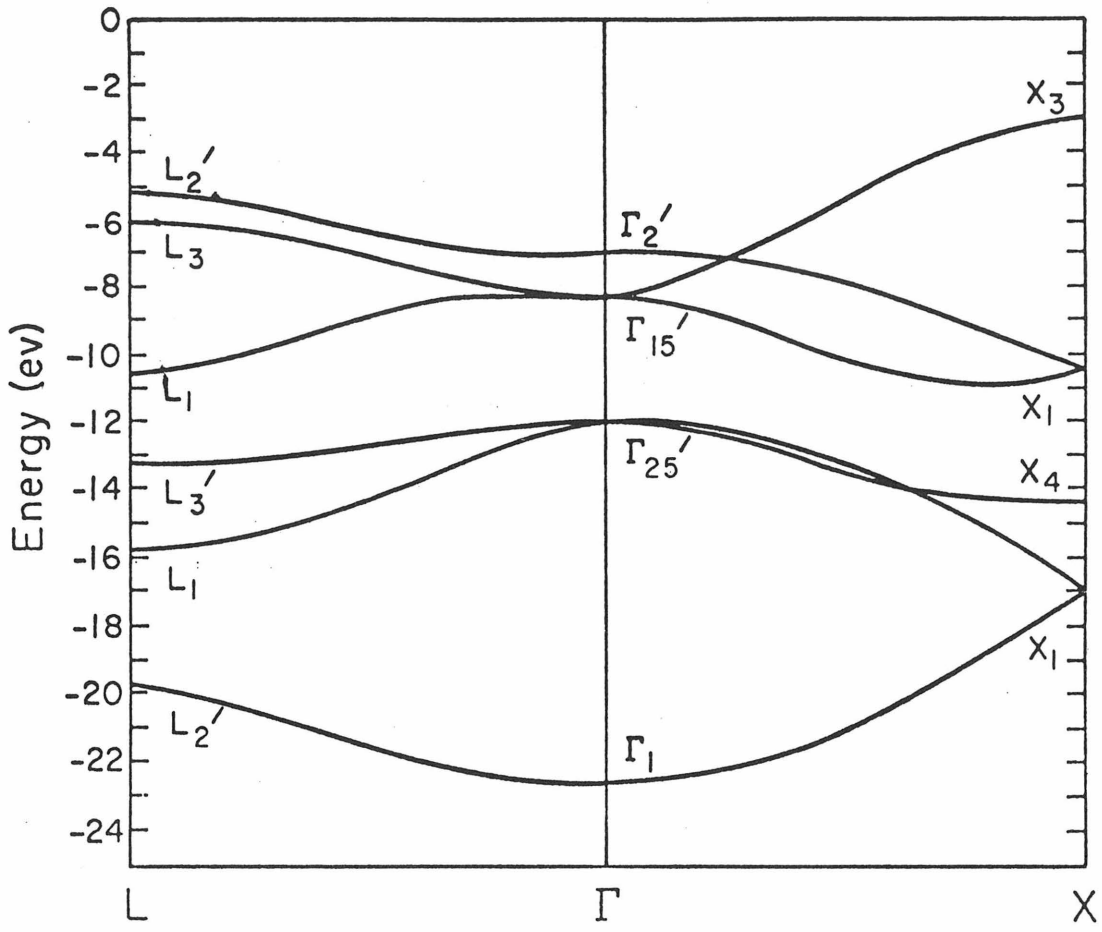

Figure 2 The band structure of silicon along Δ and Λ directions in EHT approximation. The EHT parameters: $I_{3s} = 17$, $I_{3p} = 11.6$, $K_{ss} = 1.87$, $K_{pp} = 1.81$, $K_{sp} = 1.35$. The energy gap is 1.15 eV.

3.2 Electronic Levels of Clusters

Calculations of the electronic levels of clusters of 29 and 64 atoms with no defect present show that energy levels of the cluster do not give a satisfactory representation of the electronic level structure for silicon. The electronic levels were calculated using the same EHT parameters as were used in the band structure calculation. The results of these calculations are shown in Fig. 3 where we have plotted the band structure for the large unit all at the Γ point along with the electronic levels for the 29 and 64 atom clusters. From these results, one can see that the level structure in the cluster calculation is unlike that obtained in the band structure calculation. In this figure, we have shown the location of the energy separating occupied from unoccupied levels by an arrow. For a reasonable representation of the electronic structure of the solid, we would expect there to be a region in energy just above this arrow which would be the band gap. However, as can be easily seen from Fig. 3, no such gap exists for the cases of 29 atom or 64 atom cluster.

3.3 Divacancy

We will report the results for the divacancy in two parts: first the divacancy without lattice distortion; and, second, the divacancy with lattice distortion.

3.3.1 Undistorted

The undistorted divacancy is modeled by simply removing two atoms from the center of each 64 atom unit cell (described in Sec. 2.2) in a periodic structure. The resulting unit cell has symmetry D_{3d} with the 3-fold axis of symmetry along the vector connecting the positions of the

Figure 3 a) The energy levels at the center of Brillouin zone, Γ, of Si perfect crystal with 64-atom cubic unit cell.
b) The energy levels of 64-atom cubic silicon cluster.
c) The energy levels of 29-atom silicon cluster.
The arrows indicate the level separating occupied from unoccupied levels in the case of a neutral unit.

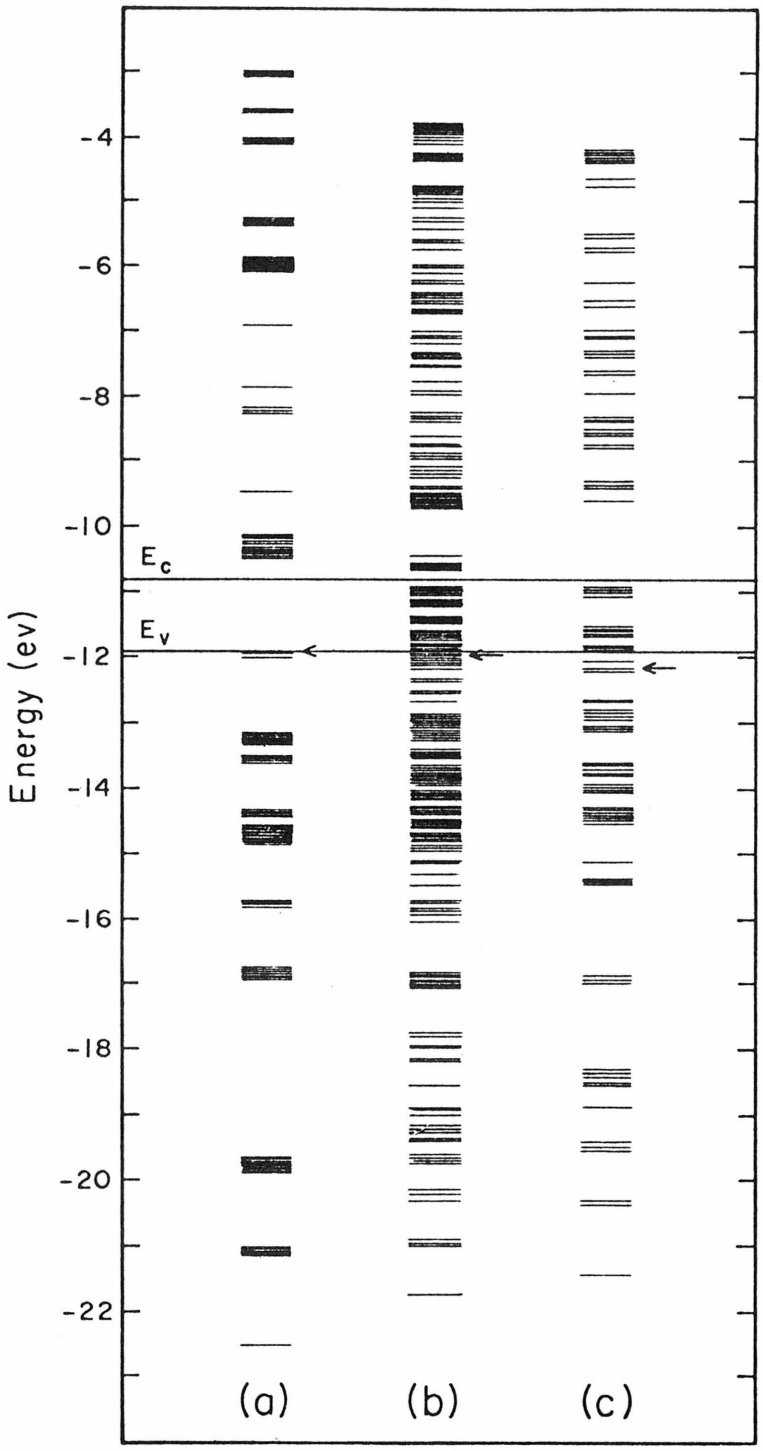
-4
-6
-8
-10
E_c
E_v
-12
-14
-16
-18
-20
-22
Energy (ev)
(a)
(b)
(c)

atoms removed to produce the divacancy. The solid produced by this procedure consists of a periodic array of oriented divacancies at a density of approximately $10^{21} cm^{-3}$ in an otherwise perfect diamond lattice.

To study the electronic levels of this large unit cell, we have made calculations of the band structure at the zone center ("Γ-point") and at the cubic Brillouin zone edge along the $(1\bar{1}0)$ direction ("M-point") oriented with respect to the divacancy as shown in Fig. 1. Each of our calculations yields 248 eigenvalues and eigenvectors. These 248 energy levels divide such that 125 are below the valence band edge for the perfect crystal and 123 levels are above. Hence, if we neglect dispersion in the eigenvalues in our small Brillouin zone, and the Fermi energy is at the valence band edge, then the unit cell contains two additional electrons above the four electrons per atom present when the cell is neutral.

We are interested in all the energy levels which are located in the energy gap and also those energy states which have large probabilities P around the divacancy (see (2.12)). Therefore we have plotted in Fig. 4 the energy levels at Γ-point and their corresponding probabilities P for all the levels in the energy gap and for the levels with P greater than 0.30. To make comparison with the results for the distorted divacancy easier, we have labeled the states with their symmetry according to C_{2h} (a subgroup of D_{3d}) (Hamermesh 1965), the symmetry of the distorted divacancy. The degeneracy of each state is indicated by the height of the line in the energy level plot. We marked in Fig. 4 the six most localized states by their symmetries. These six most localized states are also listed explicitly in the first

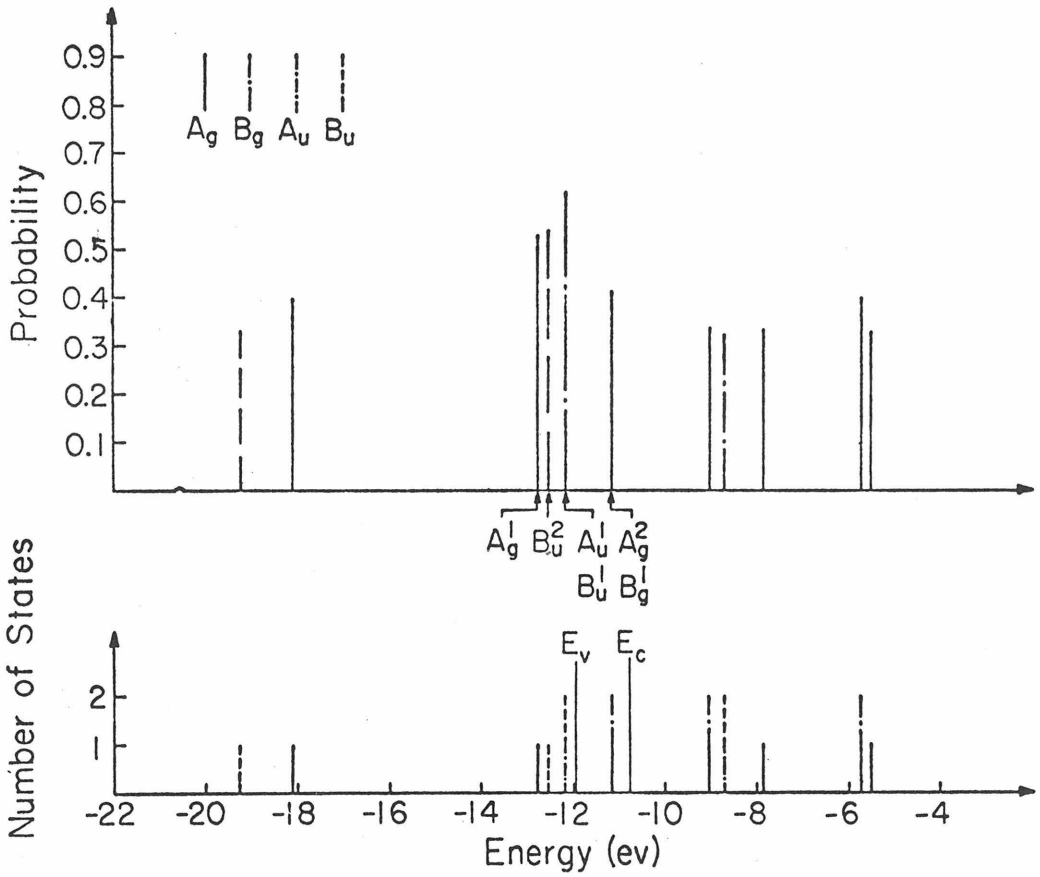

Figure 4 The energy levels of undistorted divacancy and their corresponding probabilities for all the energy states in the energy gap and the energy states with localization probabilities P greater than 0.30. The degeneracy of states is indicated by the height of the line in the energy level plot. The symmetries of the states are indicated. The six most localized states are indicated by arrows.

series of entries in Table I. Only the six most localized states were studied since these may be associated with the six dangling bonds around the divacancy (Watkins and Corbett, 1965).

Because of the rather high density of defects ($\sim 10^{21} cm^{-3}$) in our model, we have also investigated the role of defect-defect interaction. This was accomplished by computing the band structure at the above described "M-point" and again identifying the six most highly localized states. The results of this calculation are shown in the second entry in Table 1. The levels have been arranged so that they have the same symmetry as in the first entry Table 1. Comparing the two entries we see that the levels are shifted by approximately 0.2 eV and this suggests a rather strong divacancy-divacancy interaction at this density of divacancies.

To explore the use of cluster calculations which avoids the divacancy-divacancy interaction question by use of a finite number of atoms, we have made calculations for a single divacancy centered in a cluster of (62 atoms). The resulting energy of the six most highly localized states are shown in the final entry in Table 1. From these results, we see that the levels in a cluster calculation bear little resemblance in location and symmetry to those obtained in the above described calculation.

3.3.2 Distorted

The introduction of the lattice distortion discussed in Sec. 2.3 lowers the symmetry about the divacancy from D_{3d} to C_{2h} (Watkins and Corbett 1965). We have studied the influence of this lattice distortion on the energy and degree of localization of the six most highly localized

Table 1. The six most localized states at Γ with their corresponding states at M and the seven most localized states for 62-atom cluster. The probabilities of electrons being found around the divacancy are also shown here.

Γ			M($1\bar{1}0$)			Cluster		
Symmetry	Level (eV)	Probability	Symmetry	Level (eV)	Probability	Symmetry	Level (eV)	Probability
A_u^1	-12.19	61.9%	A_u^1	-12.0	46.8%	A_u^1	-4.4	49.8%
B_u^1	-12.19	61.9%	B_u^1	-12.1	59.6%	B_u^1	-4.4	49.8%
B_u^2	-12.53	54 %	B_u^2	-12.43	56.3%	A_g^1	-8.37	45 %
A_g^1	-12.79	53 %	A_g^1	-12.55	43.3%	B_g^1	-3.8	43.5%
A_g^2	-11.6	41.5%	A_g^2	-11.96	50.2%	A_g^2	-5.14	40.8%
B_g^1	-11.6	41.5%	B_g^1	-11.81	48.5%	A_g^3	-4.8	40 %

levels. In Figs. 5 and 6, we have plotted the energy and probability of being on the six nearest neighbor atoms, respectively, as a function of the lattice distortion measured by d (see Eq. (2.11)). From these figures we see that: The energy of highly localized B^1_u moves from the valence band into the energy gap. The state A^2_g increases in energy but remains in the energy gap for reasonable values of the distortion; and becomes more highly localized. The energy of the state with symmetry B^1_u remains in the energy gap but becomes more diffuse.

Turning our attention to the three states in the energy gap, the state with symmetry $B_g{}^1$ is localized around the four atoms a,d, and a',d' (See Fig. 1 for labeling of atoms around defect). The states $A_g{}^2$ and $B_u{}^1$ are localized largely on the two atoms b and b'. The best agreement between these energy eigenvalues and the experimental observed properties of the divacancy (See Sec. 4) is obtained when the distortion is 0.19 $\mathring{A}$. For the case in which the divacancy is distorted by 0.19 $\mathring{A}$, we have plotted in Fig. 7 the energy levels and the corresponding probabilities P for all the states in the energy gap and for the states with probabilities greater than 0.30. The symmetries of the states are indicated by using different symbols for different symmetries. The six states which are thought to be associated with the dangling bonds of divacancy are marked by their symmetries in Fig. 7. As we can see, most of the highly localized states are either in the energy gap or close to the top of valence band.

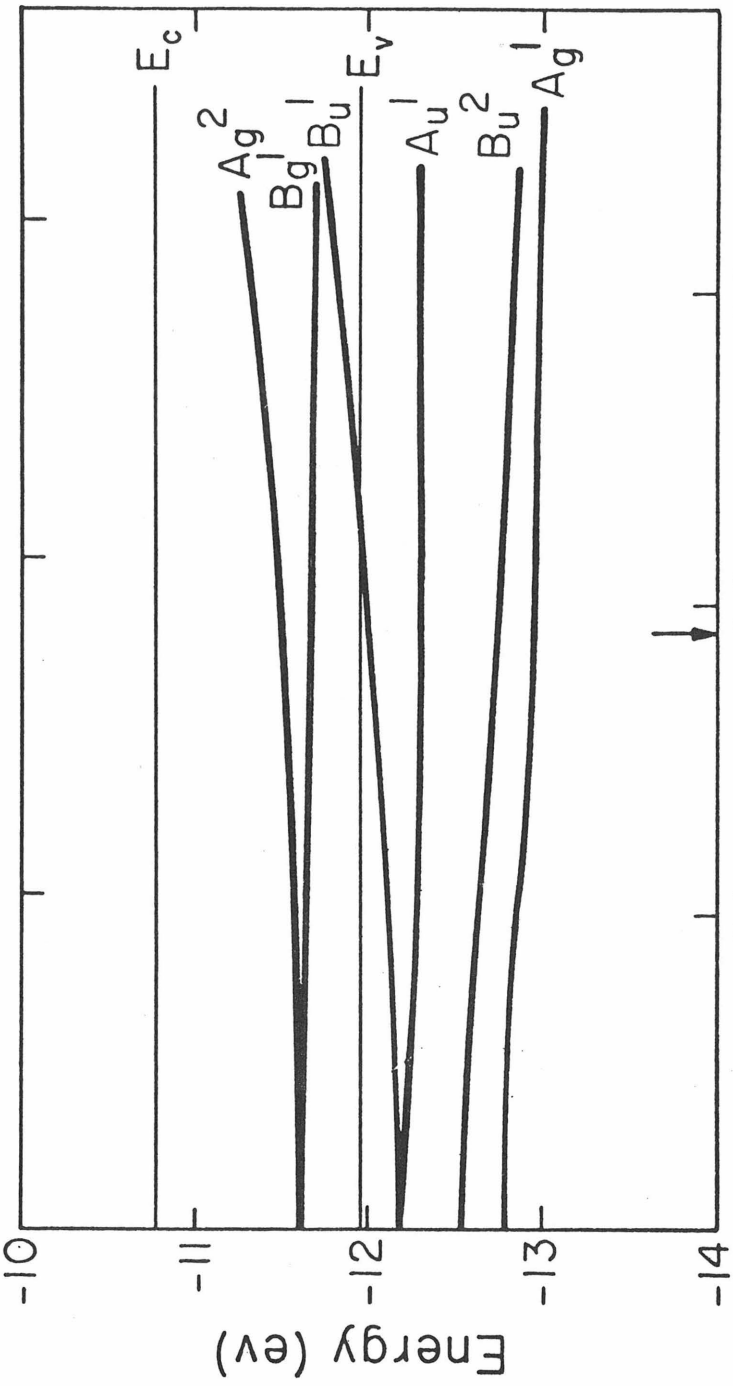

Figure 5 The variation of the six localized states as a function of distortion.

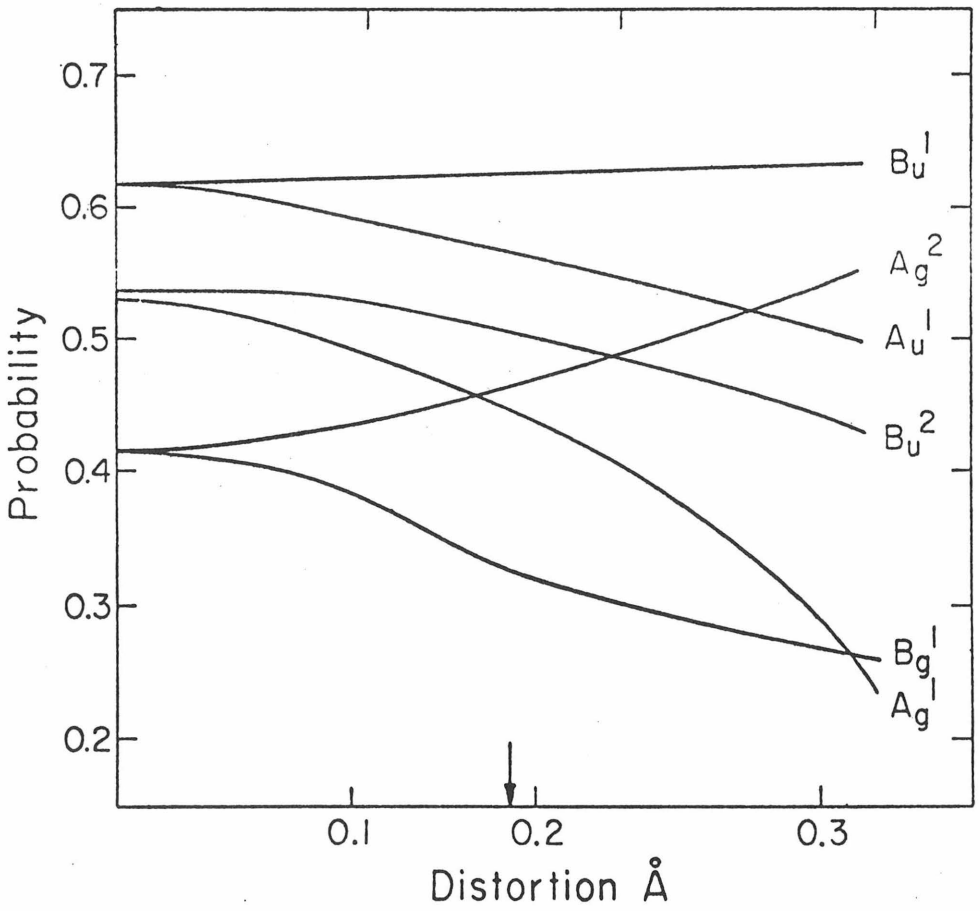

Figure 6 The probabilities of the six localized states around the six nearest atoms to divacancy.

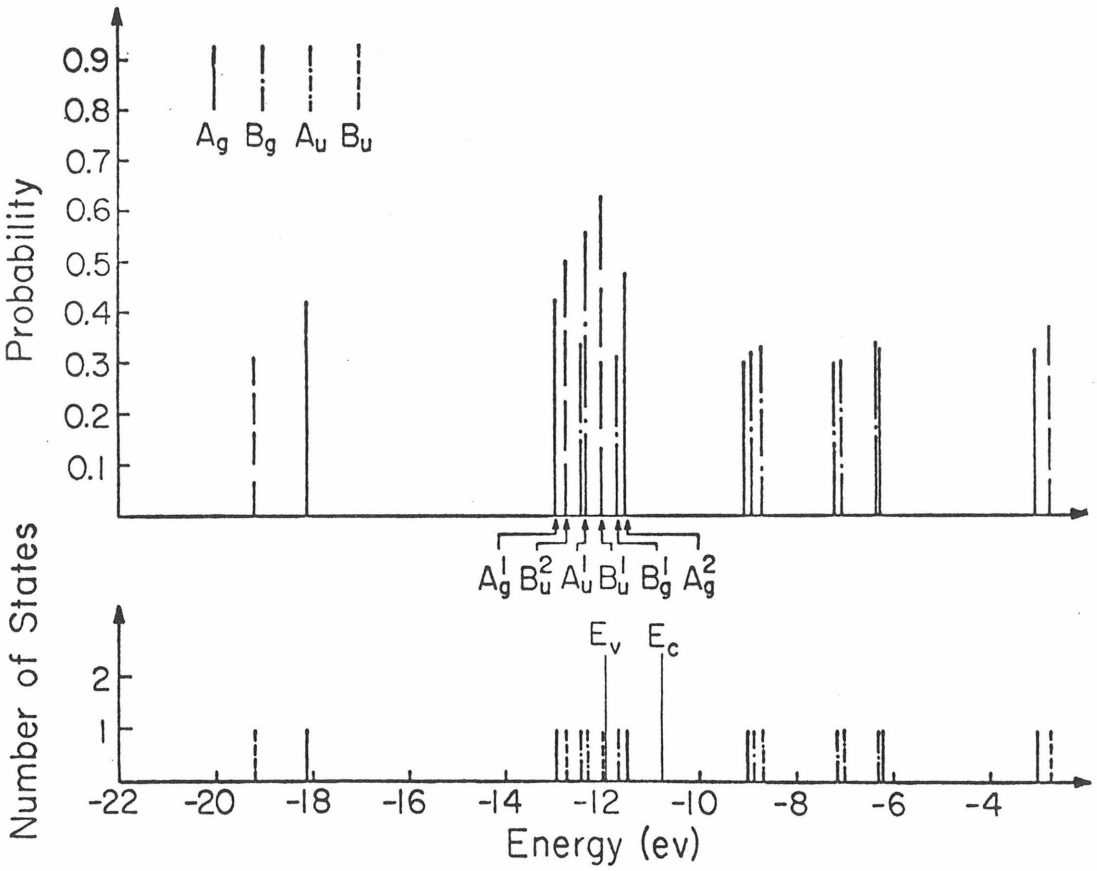

Figure 7 The energy levels of distorted divacancy and their corresponding probabilities for all the energy states in the energy gap and the energy states with localization probabilities P greater than 0.30. The symmetries of the states are indicated. The six states which are thought to be associated with the dangling bonds of divacancy are indicated by arrows.

For this value of the distortion, the 248 energy levels divide such that 124 levels are below the band edge for the perfect crystal and 124 levels are above. Hence, if we neglect dispersion in the eigenvalues in our small Brillouin zone, and the Fermi energy is at the valence band edge, then the unit cell contains four electrons per atom and is neutral.

To estimate the size of divacancy-divacancy interactions, we have also calculated the energy levels at the "M point" (see definition given above) and at the zone boundary along $(1\bar{1}1)$ direction, "R point". The results of this calculation along with the values at the Γ point for $d = 0.19$ Å are given in Table 2. As in the results for the undistorted divacancy, we note that divacancy-divacancy interaction at this density can produce level shifts which are on the order of 0.2 eV. We also note that at "R point" the B_g^1 level is in valence band and the A_g^2 and B_u^1 levels are in the energy gap. Therefore the presence of the B_g^1 level in the energy gap is uncertain; it may be due to divacancy-divacancy interactions or due to only six nearest atoms to divacancy being distorted.

4. DISCUSSION AND CONCLUSIONS

Using the extended Hückel theory (EHT), we calculated the band structure of silicon. The calculated band structure is in good agreement with the accepted band structure for silicon showing that EHT is capable of reproducing the band structure of silicon.

Table 2. The six localized states at zone center Γ and zone edge M and R when atoms deviate 0.19 Å from their original sites.

Γ			M($1\bar{1}0$)			R($1\bar{1}1$)		
Symmetry	Level (eV)	Probability	Symmetry	Level (eV)	Probability	Symmetry	Level (eV)	Probability
B_u^1	-11.98	63.3%	B_u^1	-11.97	62.1%	B_u^1	-11.86	56 %
A_u^1	-12.32	55.8%	A_u^1	-12.13	31.4%	A_u^1	-12.2	44.6%
B_u^2	-12.75	50.6%	B_u^2	-12.62	50.6%	B_u^2	-12.9	40.8%
A_g^2	-11.49	47.9%	A_g^2	-11.7	56.8%	A_g^2	-11.7	59 %
A_g^1	-12.95	42.5%	A_g^1	-12.93	45.1%	A_g^1	-12.7	33.9%
B_g^1	-11.69	31.6%	B_g^1	-11.88	42.1%	B_g^1	-12.0	51 %

Calculations of the electronic levels of free clusters of 29 and 64 atoms spatially arranged as in a perfect diamond lattice show that the electronic structure of the clusters is not the same as that of the perfect solid. If we define the top of the valence band as that energy below which half of the electronic levels occur, then the energy range from the top of the valence band to that energy plus the band gap is filled almost completely by electronic levels. This fact has necessitated our use of the large unit cell.

Using the parameters obtained in the band structure calculation, we have calculated the electronic levels for the distorted and undistorted divacancy. Labelling all the states by their symmetry in the case of the distorted divacancy, we find that the six states most highly localized about the divacancy, listed in Table 1, have the same symmetry and ordering as the six molecular states in the LCAO model proposed by Watkins and Corbett (1965). In the results presented here, the states with symmetries A_g^2 and B_g^1 are in the band gap while the remaining four states are in the valence band.

Distortion is introduced by simply moving the atoms nearest the divacancy in such a way that the symmetry around the defect is C_{2h}. This distortion produces changes in the energy of the divacancy as well as changes in the degree of localization of the states about the defect. While the distortion is very much like that invisioned by Watkins and Corbett (1965) the ordering of the states after distortion is different from that of the LCAO molecular orbital results. This result is due to interaction between the divacancy levels and the conduction or valence bands. After distortion the A^2_g level is still inside the band gap,

and the B_u^1 level has moved up into the gap; the B_g^1 levels moves downwards. The position of the B_g^1 level is uncertain since due to its more diffuse nature it is subject to greater influence by divacancy-divacancy interaction and distortion of the atoms away from the defect than the other levels. A calculation which takes account of these factors may locate the B_g' level in the valence band.

The results of these divacancy calculations are consistent with the experimental results presently available. The EPR studies of Watkins and Corbett (1965) have identified two spectral features labeled Si-G6 and Si-G7. Study of the hyperfine interactions in these spectral features has led them to conclude that about 50-60% of the total probability for an electron contributing to the EPR are localized about atoms b and b' in Fig. 1 and about 10-15% of this probability in S-like.

We interpret the Si-G6 and Si-G7 spectra as arising from single occupancy of the B_u^1, and A_g^2 levels, respectively. These two levels are in or near the band gap depending upon the degree of distortion; and 40-50% of the probabilities are found about the b and b' atoms. Furthermore, when the divacancy is distorted to equal 0.19 Å (see Eq. (2.11)), the s-wave character of the states about b and b' is about 10-15%. Both of these quantities are in reasonable agreement with the experimentally determined values.

Studies have also been made of the infrared absorption (Fan et al. 1959; Vavilov et al. 1963; Corelli et al. 1965; Cheng et al. 1966; Young et al. 1969; Chen et al. 1972) and photoconductivity (Cheng 1967, 1968; Kalma et al. 1968; Young et al. 1972) of samples containing divacancies. While there seems to be a number of contradictory experimental results, there does seem to definitely be a 1.8μ (0.69 eV) absorption in the

infrared. Experiments suggest that this absorption is due to highly localized states on the negatively charged divacancy. Group theoretical arguments suggest that this transition is between states having A_g and B_u symmetry or between states having A_u and B_g symmetry. Our theoretical calculation suggest that the transition is between our A_g^2 and B_u^1 states. The calculated energy difference is 0.5 eV, which is reasonable agreement with the 0.69 eV observed. We have been unable to identify the number of other transitions reported by various authors.

In conclusion, the extended Hückel theory combined with periodic boundary conditions induced by using a large unit cell gives results in qualitative agreement with the experimental results available.

REFERENCES

Bennemann K H 1965 Phys. Rev. 137 A1497-514.

Callaway J 1964 J. Math Phys. 5 783-98.

Callaway J and Hughes A J 1967 Phys. Rev. 164 1043-9.

Chen C S and Corelli J C 1972 Phys. Rev. B5 1505-17.

Cheng L J 1967 Phys. Lett. 24A 729-31.

-----1968 in Radiation Effects in Semiconductors ed F L Vook (New York: Plenum) 143-51.

Cheng L J, Corelli J C, Corbett J W, and Watkins G D 1966 Phys. Rev. 152 761-74.

Clementi E 1965 Suppl IBM J. Res. Dev. 9 2 Table 01-06.

Corelli J C, Oehler G, Becker J F, and Eisentraut K J 1965 J. Appl. Phys 36 1787-8.

Coulson C A and Kearsley M J 1957 Proc. Roy. Soc. A241 433-53.

Coulson C A and Larkins F P 1969 J. Phys. Chem Solids 30 1963-72.

-----1971 J. Phys. Chem. Solids 32 2245-57.

Fan H Y and Ramadas A K 1959 J. Appl. Phys. 30 1127-34.

Hamermesh W 1962 Group Theory and Its Application to Physical Problems (New York: Addison Wesley Publishing Company, Inc.) 125-26.

Herman F et al. 1966 Quantum Theory of Atoms, Molecules, and the Solid State ed P Lowdin (New York: Academic Press, Inc.) 381-428.

Hoffman R 1963 J. Chem. Phys. 39 1397-412.

Kalma A H and Corelli J C 1968 Phys. Rev. 173 734-45.

Kohn W 1957 Solid State Phys. ed F Seitz and D Turnbull (New York: Academic Press) 5 257-320.

Larkins F P 1971a J. Phys. Chem Solids 32 2123-8.

-----1971b J. Phys. Chem. Solids 4 3065-76.

-----1971c J. Phys. Chem. Solids 4 3077-82.

Messmer R P 1971 Chem. Phys. Letters 11 589-92.

Messmer R P and Watkins G D 1970 Phys. Rev. Lett. 25 656-9.

-----1971 Radiation Effects 9 9-14.

Vavilov V S, Plotnikov A F, and Tkachev V D 1963 Sov. Phys. Solid State 4 2522-8.

Watkins G D 1968 Radiation Effects in Semiconductors ed F L Vook (New York: Plenum) 67-81.

Watkins G D and Corbett J W 1965 Phys. Rev. 138 A543-55.

Watkins G D and Messmer R P 1970 Proceedings of the Tenth International Conference on the Physics of Semiconductors, Cambridge, Massachusetts ed S P Keller, J C Hensel, and F Stern (U.S. Atomic Energy Commission Oak Ridge Tennessee) 623-7.

Young R C and Corelli J C 1972 Phys. Rev. B5 1455-67.

Young R C, Westhead J W, and Corelli J C 1969 J. Appl. Phys. 40 271-8.

PART THREE

VARIATION OF IMPURITY-TO-BAND ACTIVATION ENERGIES WITH IMPURITY DENSITY

I. INTRODUCTION

Since the work of Pearson and Bardeen[1] in 1949, it has been well known that the impurity-to-band activation energy in semiconductors decreases with increasing impurity concentrations. At low impurity concentrations (for example, less than 10^{17} phosphorus/cm^3 in silicon), the variation of activation energy with impurity concentrations is small. At high-impurity concentrations, the activation energy is strongly dependent upon the impurity concentrations. A number of different suggestions have been put forward to account for this phenomenon theoretically. Pearson and Bardeen[1], and Castellan and Seitz[2] suggested that the decrease of impurity-to-band activation energy with impurity concentrations was due to attraction between the conduction electrons and ionized donors. Calculations based upon this physical phenomenon yielded qualitative but not quantitative agreement with the experimental results. Pincherle[3] proposed that free carriers screen the field of the impurity center and hence decrease the binding energy of a carrier electron to an impurity center. Calculation based on this proposal alone did not give satisfactory results. A self-consistent calculation which combined the two models was given by Lehman and James.[4] While this calculation was in good agreement with experiment for low impurity concentrations, at high impurity concentrations ($10^{16}cm^{-3}$ shallow donors in Ge), their calculations underestimate the experimentally observed decrease of activation energy. A more systematic treatment proposed by Debye and Conwell[5] suggested that a correct description would include three effects - (i) lowering of the conduction band edge due to attraction of the conduction electrons by the ionized donors, (ii) the shift of the

donor ground state energy due to free electron screening, and (iii) the increase in the dielectric constant due to the presence of the polarizable neutral donors. As in the case of Lehman and James they obtain good agreement with experiment at low impurity concentrations. None of these authors has considered the role of phenomenon which would lead to impurity broadening and hence change the observed activation energy.

In this paper we consider the change in the observed activation energy due to the influence of those effects which both broaden and shift the impurity level. We consider the same phenomenon which tend to shift the level as considered by Debye and Conwell. We have included two effects which tend to broaden the level. First, the impurity level wavefunction at a given impurity has finite Hamiltonian matrix elements with impurity level wavefunctions centered at nearby impurities. This leads to broadening of impurity levels when the impurities are at finite density to produce a band of levels. Second, the presence of charged impurities distributed in a random way throughout the solid generates potential fluctuations. These potential fluctuations produce tailing of conduction and valence band density of states[6] and spreading of impurity levels.[7] For simplicity, we will confine our attention to shallow donor levels with compensating acceptors in silicon.

This paper is organized in the following fashion. In Section II, we consider those phenomena which shift the energy level. In this section, we review the results of Lehman and James and put the formulas in a form suitable for our use. In Section III, we consider the conduction band edge tailing effect due to potential fluctuations. In Section IV, the phenomena

which broaden the impurity level are investigated. Section V contains the calculations of conduction electron concentration n versus temperature T for various donor and compensating acceptor concentrations and compare the calculated results with the known experimental results. Section VI contains a brief discussion and conclusions.

II. IMPURITY LEVEL SHIFT WITH RESPECT TO CONDUCTION BAND EDGE

In the effective mass theory approximation, the Hamiltonian for the conduction electrons consists of electron kinetic energies, electron-impurity Coulomb interactions and the electron-electron interactions. Once the electron is bound the donor ion plus electron becomes a neutral system and has little effect on the motion of conduction electrons. Hence the unbound electron motion can be accurately described by a Hamiltonian which does not include any interaction with these neutral systems. The motion of conduction electrons can be approximately described by a series of one-electron Hamiltonian[8,9]

$$H = \frac{p^2}{2m^*} + \sum_{\beta}{}' \frac{Z_\beta q^2 e^{-\frac{|\vec{r}-\vec{R}_\beta|}{\lambda_e}}}{4\pi\varepsilon\varepsilon_o|\vec{r}-\vec{R}_\beta|} \quad , \qquad \text{(II-1)}$$

where $\vec{r}$ and $\vec{p}$ are the position and momenum, respectively, of the electron; $\vec{R}_\beta$ is the position of the β^{th} impurity which has signed charge Z_β; the prime above the summation indicates that the sum runs over ionized impurities only. The semiconductor is described by an isotropic effective mass m^* and dielectric constant ε. The electron screening length is λ_e. For non-degenerate case, the electron screening length is given by[10]

$$\lambda_e = \sqrt{\frac{\varepsilon\varepsilon_o K_B T}{q^2 n}} \quad , \qquad \text{(II-2)}$$

where n is conduction electron concentration, K_B is Boltzmann constant, and T is absolute temperature. For silicon, λ_e ranges typically between 40 Å and 10^4 Å for $n = 10^{18}\text{cm}^{-3}$ and $T = 300°\text{K}$, and for $n = 10^{12}\text{cm}^{-3}$ and $T = 50°\text{K}$, respectively. We will use the Hamiltonian in Eq. (II-1) to describe the unbound conduction electrons.

There are several effects which are thought to be related to the shift of impurity levels with respect to the conduction band edge. They are: (i) the change of dielectric constant due to the presence of neutral donors, (ii) the influence of conduction electron screening on donor ground state energy, and (iii) the conduction band edge lowering due to attraction between conduction electrons and ionized donors. In the following, we are going to examine these three effects.

A. Neutral Donor Polarization

In Eq. (II-1), there is some question about what dielectric constant we should use. As pointed out by Castellan and Seitz,[2] we should include the contribution to ε due to the presence of polarizable neutral donors. However, this produces a small change in ε. For donor concentrations up to 10^{18} neutral-donors/cm^3, the concomitant shift of impurity energy level relative to the conduction band edge is less than 1 meV. Hence, we will assume that the dielectric constant is independent of impurity concentrations.

B. Shift of Impurity Level to Screening

The presence of the conduction electrons should screen the attractive interaction between the donor ion and the bound electron in a donor level. This screening will tend to shift the donor ground state energy toward the conduction band. Using Hartree approximation, Lehman and James[4] had included this effect in their self-consistent calculation. For the purpose of estimating the size of this effect and to separate this effect from the conduction band edge shift effect, we will make a simple first order perturbation calculation of this effect. We approximate the donor ground state wavefunction by a single 1s Slater orbital with an exponent of ξ. The potential due to the conduction electrons is obtained by computing the change in local electron density due to the presence of the donor ion and the bound electron in a linearized Hartree approximation.

Since the electron screening length is larger than the size of the donor level wavefunction, i.e. $\xi\lambda_e > 1$, the difference between the screened ion potential and the unscreened ion potential is small. First order perturbation theory of this difference potential can be used to estimate the shift in the donor level due to conduction electron screening. The result of the calculation is

$$\Delta E_B \equiv \frac{q^2\xi}{4\pi\epsilon\epsilon_0}\left\{\frac{3}{8} - \frac{2\,\xi\lambda_e \sin\left[\frac{1}{2\xi\lambda_e} + 2\tan^{-1}\frac{1}{8\xi\lambda_e}\right]}{4 + \frac{1}{16\xi^2\lambda_e^2}}\right\} \quad , \qquad \text{(III-3)}$$

(see the Appendix for a derivation of this result). ΔE_B is a monotonically decreasing function of the screening length λ_e, we can obtain

an upper bound to ΔE_B by taking the smallest value of λ_e that we encountered under the present experimental conditions (about 40 Å). Taking ξ to be the reciprocal of the Bohr radius for the donor $\left(\xi = \frac{1}{19\text{Å}}\right)$ in Si , we have that

$$\Delta E_B \leq 1 \text{ meV} \quad ,$$

for conduction electron concentrations less than $10^{18} cm^{-3}$ in Si. This result agrees with the calculations of Lehman and James which indicated that screening produced a small impurity level shift. Therefore, we can neglect the effect of screening on the donor ground state energy level.

C. Average Shift of Conduction Band Edge

The presence of ionized donors and compensating acceptors changes the position of the conduction band edge. The random spatial distribution of the ionized centers leads to not only an average shift of the conduction band edge but also spatial fluctuations in the position of the conduction band edge. In this section we concentrate on the average shift of the conduction band edge and leave to a later section the discussion of fluctuations.

To make an estimate of the average shift, we should in principle calculate the energy levels associated with the potentials due to the ionized impurities, then devise some method of defining the bottom of the conduction band, and finally average this over all the possible spatial configurations of ionized impurities. While this is in principle the way to proceed, in practice we can not carry out such a calculation

in anything but the most idealized models. Thus, we proceed by first obtaining a potential which should approximate the potential due to the ionized impurities. In obtaining the potential due to a single ionized donor, the principal dopant, we must note that the Coulomb potential of a donor is modified by the presence of the conduction electrons and also by the increased probability of finding an ionized acceptor near an ionized donor. These two effects are taken into account by screening the Coulomb potential of the donor. The screening length is made up of two parts - that due to the electrons, and that due to the ionized impurities. The screening length for the electrons is the same as that given before in Eq. (II-2). The screening length for ionized impurities is given by a standard Debeye screening length form (λ_i)[11,12] modified by the addition of a length which is the average spacing between impurities.[7] That is,

$$\lambda_i = \lambda_{io} + a \quad , \qquad \text{(II-4)}$$

where

$$\lambda_{io} = \sqrt{\frac{\varepsilon\varepsilon_o \, k_B \, T/q^2}{(N_A+n)\left(1 - \frac{N_A+n}{N_D}\right)}} \quad , \qquad \text{(II-5)}$$

and

$$a = 0.893 \left(\frac{4\pi}{3}(N_D + N_A)\right)^{-1/3} \quad , \qquad \text{(II-6)}$$

which is the average distance under Poisson distribution. The total screening length λ is given by

$$\lambda^{-2} = \lambda_e^{-2} + \lambda_i^{-2} \quad . \quad \text{(II-7)}$$

With this screening length the potential about a donor becomes

$$V(\vec{r}) = \frac{-q^2 e^{-r/\lambda}}{4\pi\varepsilon\varepsilon_0 r} \quad . \quad \text{(II-8)}$$

To estimate the average lowering of the conduction band edge, we concentrate our attention on the potential between two impurities which are separated by the average distance between donors. The average shift can be divided into two parts. First, the conduction electron barrier height is lowered due to the overlap of the potential of ionized donors as illustrated in Fig. 1. Second, the conduction band edge actually occurs somewhat below the maximum of the potential due to electron tunneling. We first calculate the maximum of the potential. If only the nearest neighbor is considered, the lowering of the barrier height as shown in Fig. 1 is approximately equal to

$$\Delta E_{1c} \simeq \frac{2q^2 e^{-\frac{d}{2\lambda}}}{4\pi\varepsilon\varepsilon_0 (d/2)} - \frac{q^2 e^{-\frac{d}{\lambda}}}{4\pi\varepsilon\varepsilon_0 d} \quad ,$$

with $d = (N_D^+)^{-1/3}$ where N_D^+ is the ionized donor concentration. The first term in (II-9) corresponds to the potential lowering at the middle point of the two nearby ionized donors. The second term corresponds to the potential lowering at the ionized donor site due to the presence of the nearby ionized donor.

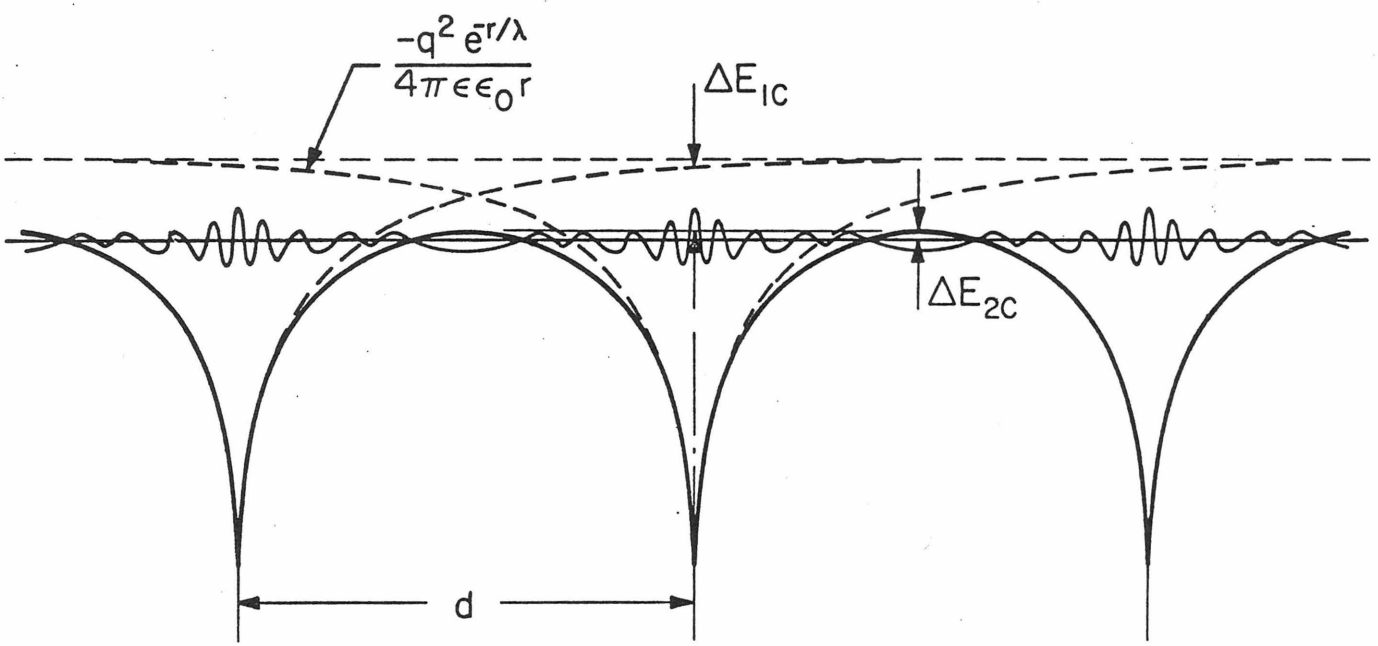

Fig. 1 The shift of conduction band edge due to overlap of ionized donor potentials. The lowering of barrier height is ΔE_{1c} and the total shift of conduction band edge is $\Delta E_{1c} + \Delta E_{2c}$.

As we have mentioned above, because of electron tunneling the conduction band edge occurs below the maximum in the potential. The location of the average conduction band edge depends upon the shape of the ionized donor potential. We have made a rough estimate about the location of the conduction band edge measured with respect to the maximum in the potential $(-\Delta E_{2c})$, and found that it is small for the cases considered here. Therefore, we can use the result of the rough estimate and it will not introduce significant error in our calculation. The estimate proceeds as follows. We assume that the excited donor state is an extended state if the average radius of the electron wavefunction of the excited state is half the distance between ionized donors. We also assume that as r becomes large the electron wavefunction of the excited state approaches to

$$\phi_n(\vec{r}) \propto e^{-Kr} \quad , \qquad \text{(II-9)}$$

where $K \equiv \sqrt{\frac{2m^* \Delta E_{2c}}{\hbar^2}}$ and $(-\Delta E_{2c})$ is the bottom of conduction band measured with respect to the top of the potential barrier. Hence the average radius of the electron wavefunction is approximately equal to $(K)^{-1}$. Setting the average radius of the electron wavefunction to equal to the half distance between ionized donors, i.e. $(K)^{-1} = d/2$. we have

$$\Delta E_{2c} = \frac{2\hbar^2}{m^* d^2} \quad . \qquad \text{(II-10)}$$

The total downward shift of the conduction band edge is thus equal to

$$\Delta E_c = \Delta E_{1c} + \Delta E_{2c} \quad . \quad \text{(II-11)}$$

For the donor concentrations and temperatures we are interested in, ΔE_c gives significant contribution to the decrease of activation energy, as will be shown in Section V.

III. CONDUCTION BAND EDGE TAILING

Donors and acceptors are approximately randomly distributed in the semiconductors. The random distribution of ionized donors and acceptors generates spatial fluctuations in the potential. The potential fluctuation smear out the conduction band edge and thus produce a tail on the conduction band density of states.[6]

The work of Kane[6] and Morgan[7] indicates that the distribution of potential $p(v)$ is approximately Gaussian,

$$p(v) = \frac{1}{\sqrt{2\pi}\,\sigma} e^{-v^2/2\sigma^2} \quad , \quad \text{(III-1)}$$

with a standard deviation σ given by

$$\sigma = \left[\frac{(N_D^+ + N_A)}{8\pi^2 \varepsilon^2 \varepsilon_o^2} q^4 \lambda \right]^{1/2} \quad , \quad \text{(III-2)}$$

where λ is the screening length which is given by Eq. (II-7). This distribution of potential fluctuations generates a tail on the conduction band density of states which extends to minus infinity in energy. However, the mobility of electrons in the density of states tail is a function of energy, approaching zero for energies below a certain energy in the tail.

For simplicity, we will assume that the mobility is constant for energies greater than -2σ and that the mobility is zero for energies less than -2σ. Hence, states with energy less than -2σ do not contribute to the conduction since their mobility is zero.

For slowly varying potential fluctuations, the local density of states at a point with potential v is given by

$$\rho_c(E) = \frac{6\sqrt{2}\,(m^*)^{3/2}}{\pi^2\hbar^3}\,(E-v)^{1/2} \quad . \qquad \text{(III-3)}$$

The average conduction band density of states is given by

$$N_c(E) = \begin{cases} \displaystyle\int_{-\infty}^{E} \rho_c(E-v)p(v)dv & E \geq -2\sigma \\ 0 & E < -2\sigma \end{cases} \quad . \qquad \text{(III-4)}$$

The magnitude and extend of the conduction band density of states depends upon the value of σ . For typical values of the parameters, σ can attain values of as large as 10 meV (see discussion in Sec. V). Hence, the broadening of the conduction band edge can lead to significant effects on the observed activation energy.

IV. BROADENING OF DONOR LEVEL

There are two effects which tend to broaden the level. First, the localized wavefunction of the impurity level at a given impurity has finite Hamiltonian matrix element with localized wavefunctions centered at nearby impurities. At finite densities, this leads to broadening of impurity

levels into a band of levels. Second, the potential fluctuations due to random distribution of charge impurities lead to changes in the energy of the various localized impurity states.

A. Level Broadening Due to Donor Wavefunction Overlap

For one single isolated shallow donor, such as P, As, or Sb in Si, the hydrogenic model can be applied to define the donor energy state. For semiconductors with shallow donor concentration N_D, the donor ground state level is discrete but has N_D-fold degeneracy if there is no interaction between the donor impurities. However, if there are finite Hamiltonian matrix elements between the donor ground state wavefunctions on different sites, the degeneracy is lifted and the single donor ground energy is broadened into a band. If the overlaps between the donor ground state wavefunctions at different sites are small, we can use tight binding model to estimate the donor level broadening. In this model, the donor level broadening is proportional to the energy transfer integral,[13]

$$J(|\vec{R}_i-\vec{R}_j|) = \int \frac{q^2}{4\pi\varepsilon\varepsilon_o\,|\vec{\gamma}-\vec{R}_i|}\ \phi_o(\vec{\gamma}-\vec{R}_i)\ \phi_o(\vec{\gamma}-\vec{R}_j)\ d^3\gamma \quad , \tag{IV-1}$$

where $\phi_o(\gamma)$ is donor ground state wavefunction. Using scaled hydrogenic model for donor ground state wavefunction, we have

$$\phi_o(\vec{\gamma}-\vec{R}_i) = \sqrt{\frac{\xi^2}{\pi}}\ e^{-\xi|\vec{\gamma}-\vec{R}_i|} \quad , \tag{IV-2}$$

with $\xi = \frac{1}{a_H}\sqrt{\frac{E_D}{E_o}}$, where $(-E_D)$ is the donor ionization energy for the

low donor concentration case and $E_o \equiv -\frac{q^2}{8\pi\epsilon\epsilon_o a_H}$ is the ground state energy calculated from effective mass theory.[14] With $\phi_o(\vec{\gamma})$ given in (IV-2), the integration in (IV-1) can be carried out and leads to

$$J(R) = \frac{q^2\xi}{4\pi\epsilon\epsilon_o}\ (1 + \xi R)\ e^{-\xi R} \quad , \qquad \text{(IV-3)}$$

where R is the distance between nearest donor neighbors. As shown in (IV-3), the energy transfer integral $J(R)$ depends exponentially on the nearest donor neighbor distance R. Since the donors are randomly distributed in space, the distance R to the nearest donor neighbor and the energy transfer integral $J(R)$ varies from one donor site to the next. If the donors are absolutely randomly distributed in semiconductors, they should follow a Poisson distribution. In a Poisson distribution, the probability that the nearest donor neighbor lies in a distance R in a spherical shell between R and $R + dR$ is given by

$$4\pi N_D \exp\left(-\frac{4\pi}{3} N_D R^3\right) R^2\, dR$$

Therefore, the average energy transfer integral between a donor and its nearest donor neighbor is equal to

$$\langle J(R)\rangle = \int J(R)\cdot 4\pi N_D R^2 \exp\left(-\frac{4\pi}{3} N_D R^3\right) dR \quad . \qquad \text{(IV-4)}$$

In the tight binding model, the total band width B is equal to $2z|\langle J(R)\rangle|$ where z is the number of nearest neighbors. With a Poisson distribution, there is only one nearest neighbor to every donor and therefore z is equal to 1. Hence the total band width B is given by

$$B = 2|< J(R) >| \qquad . \qquad \text{(IV-5)}$$

The quantity of importance in our calculation is the impurity band density of states $\rho_o(E)$. In general, this is a very complicated function of energy. However, for purposes here it suffices to take $\rho_o(E)$ to be a constant over the bandwidth B. That is, if we take to midband to occur at zero energy, then

$$\rho_o(E) = \begin{cases} \frac{N_D}{B} & -\frac{B}{2} \leq E \leq \frac{B}{2} \\ o & \text{otherwise} \end{cases} \qquad . \qquad \text{(IV-6)}$$

We found for example, that for $10^{18}cm^{-3}$ shallow donors the donor band width is about 30 meV. Thus, this broadening of the impurity energy level is one of the important effects which have to be included when considering the variation of activation energies as a function of impurity concentration and temperature.

B. Level Spreading Due to Potential Fluctuation

As we have mentioned in Section III, the random distribution of ionized donors and acceptors generates spatial fluctuations in the potential. If the local potential varies slowly over the size of the wavefunction, an assumption which is true for the cases considered here, then the donor ground states vary along with the potential fluctuations. Therefore, the impurity states are spread in energy[7].

The donor level density of states $\rho_i(E)$ which is appropriate to our calculation should include both the fluctuation induced broadening

and the broadening due to the energy transfer integral. These two effects can be combined by averaging $\rho_0(E)$ given in Eq. (IV-6) over the value of the local potential. That is,

$$\rho_i(E) = \int_{-\infty}^{+\infty} \rho_0(E-v)p(v)dv \quad , \qquad \text{(IV-7)}$$

where $p(v)$ is given by Eq. (III-1).

V. CALCULATIONS AND COMPARISON WITH EXPERIMENTAL RESULTS

One way to obtain the impurity activation energy in a semiconductor is to study the conduction electron concentration as a function of temperature (Arrehnus plot). Therefore, in this section we are going to use the results of previous sections and calculate the conduction electron concentrations as a function of temperature.

The conduction electron concentration is given by the standard expression

$$n = \int_{-\infty}^{\infty} \frac{N_c(E)\, dE}{1 + \exp\left(\frac{E-E_f}{K_B T}\right)} \quad , \qquad \text{(V-1)}$$

where $N_c(E)$ has been defined in Eq. (III-4) and E_f is the Fermi energy. Similarly, the concentration of ionized donors is defined as

$$N_D^+ = \int_{-\infty}^{\infty} \frac{\rho_i(E-E_D')\, dE}{1 + g \exp\left(\frac{E_f-E}{K_B T}\right)} \quad , \qquad \text{(V-2)}$$

where $\rho_i(E)$ is defined in (IV-7) and g is degeneracy factor; E_D' is

the center of the impurity band and is related to the donor ionization energy of very dilute system, $(-E_D)$, by

$$E_D' = E_D + \Delta E_c \quad , \qquad \text{(V-3)}$$

with ΔE_c defined in (II-11). Charge neutrality leads to

$$n + N_A = N_D^+ \quad , \qquad \text{(V-4)}$$

which determines the Fermi level E_f and, in turn, the electron concentration can be obtained from (V-1). It should be noted that $\rho_i(E)$ and $N_c(E)$ are functions of σ and σ is a function of n and N_D^+. Hence, n and N_D^+ have to be solved self-consistently.

To illustrate these analytical results, we have made numerical calculations of n versus T for shallow donor in silicon (for example P , As, and Sb). The values of ε and m^* were taken to 11.8 and 0.33 m_e, respectively. The degeneracy factor was taken to be 2. In Fig. 2, the calculated n versus the reciprocial of T is plotted for different P concentrations. The compensation ratios K, ratio of acceptors to donors, is fixed at 0.5% and the ionization energy of P in Si at low concentrations is taken to be 44meV.[15] At this rather small value of compensation ratio the presence of compensation centers is relatively unimportant. The activation energy is proportional to the slope of Arrehnus plot. We see that as P concentration increases the slope and hence the activation energy decreases as expected.

To gauge the relative importance of the various phenomena in this case, we have calculated the values of the ΔE_c, B, and σ at two different temperatures 200°K and 25°K. These results are given in Table I. From

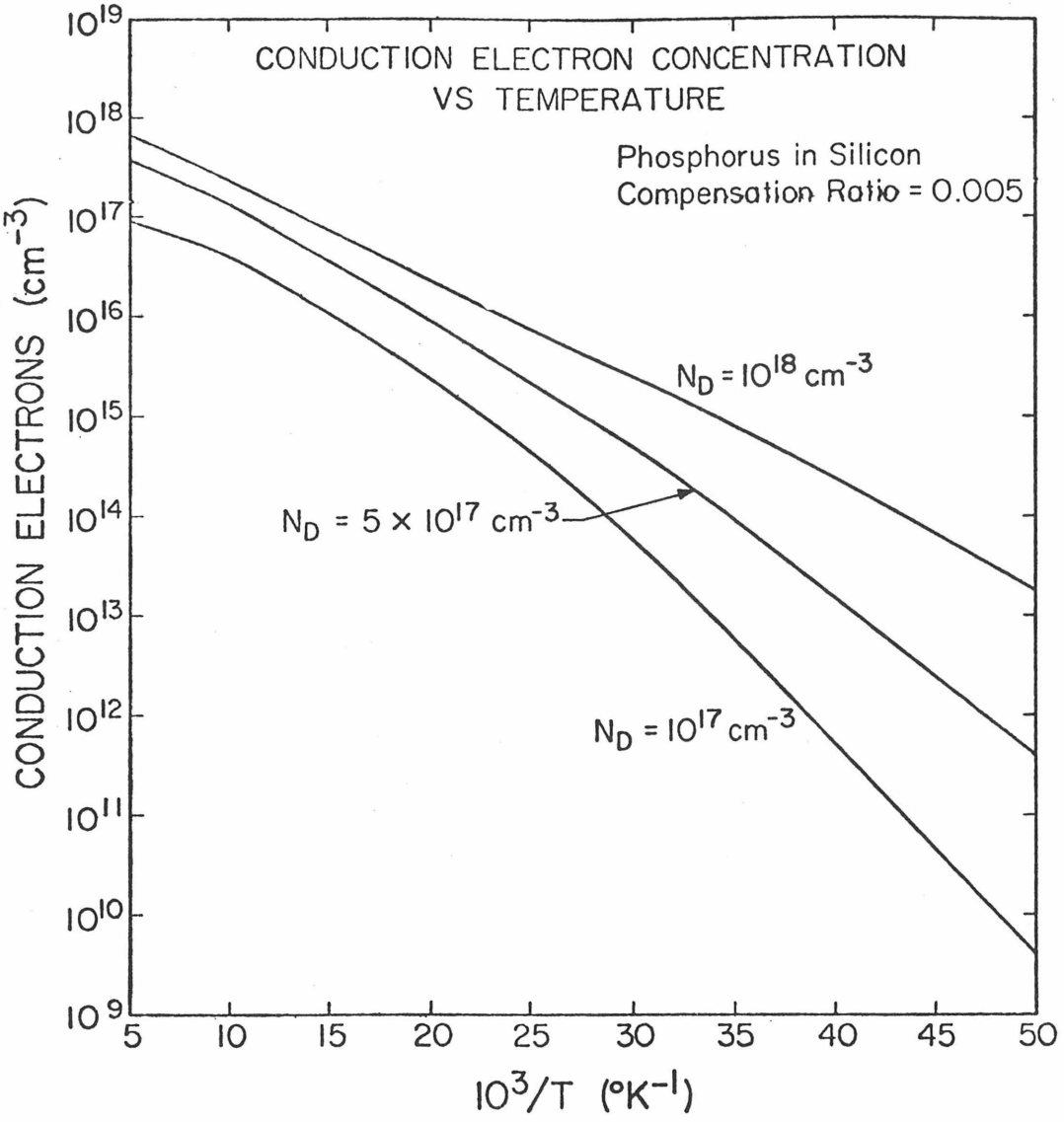

Fig. 2 The conduction electron concentration versus reciprocal temperature for different phosphorus concentrations in silicon. The compensation ratio is 0.5%.

Table I. Values for ΔE_c, B, and σ for different donor concentrations and temperatures. The compensation ratio is 0.5%

N_A and N_D (cm^{-3})	T (°K)	n (cm^{-3})	ΔE_c (meV)	B (meV)	σ (meV)
$N_A = 5 \times 10^{14}$	25	5.17×10^{11}	1.36	5.58	2.47
$N_D = 10^{17}$	200	9.06×10^{16}	8.14	5.58	9.59
$N_A = 2.5 \times 10^{15}$	25	1.52×10^{13}	1.93	19.3	3.79
$N_D = 5 \times 10^{17}$	200	3.73×10^{17}	11.3	19.3	13.6
$N_A = 5 \times 10^{15}$	25	2.47×10^{14}	2.17	29.8	4.48
$N_D = 10^{18}$	200	6.59×10^{17}	13.1	29.8	15.7

this table, we note that ΔE_c varies by a factor of 4 to 7 between 200°K and 25°K. This is due to the variation in the number of unoccupied donors and hence the potential a free electron in the conduction band sees. The value of B varies from 5.6 meV at the low concentration of $10^{17}cm^{-3}$ to 29.8 meV at the high concentration of $10^{18}cm^{-3}$. This variation is due to the increase in the energy transfer integral with increasing donor concentrations. The value of σ also shows a considerable variation with temperature and a small variation with donor concentration. The large variation with temperature is due to freeze out of the conduction electrons to the ionized donors.

To investigate the effect of compensation centers on the activation energy, we have calculated conduction electron concentrations versus 1/T for fixed P concentration with different compensation ratios. The results for P concentrations of $5 \times 10^{17}cm^{-3}$ are given in Fig. 3. This figure shows that as K increases the slope and hence the activation energy decrease. To show the relative importance of the various phenomena in this case, we have calculated the values of ΔE_c, B, and σ at two different temperatures, 25°K and 200°K, and listed the results in Table II. Since ΔE_c is primarily a function of N_D, we note little variation in ΔE_c with changes in K in this range. Again ΔE_c shows a rather large variation with temperature because of the "freeze out" of the conduction electrons. As expected B shows no variation with K since it is a function of the donor concentration only. The values of σ show a small increase with K at fixed T since the magnitude of the fluctuations in the potential increase with increasing compensation. The variation of σ with T is again due to the "freeze out" of the conduction electrons. As K increases, the conduction band edge lowering ΔE_c and potential fluctuation σ are

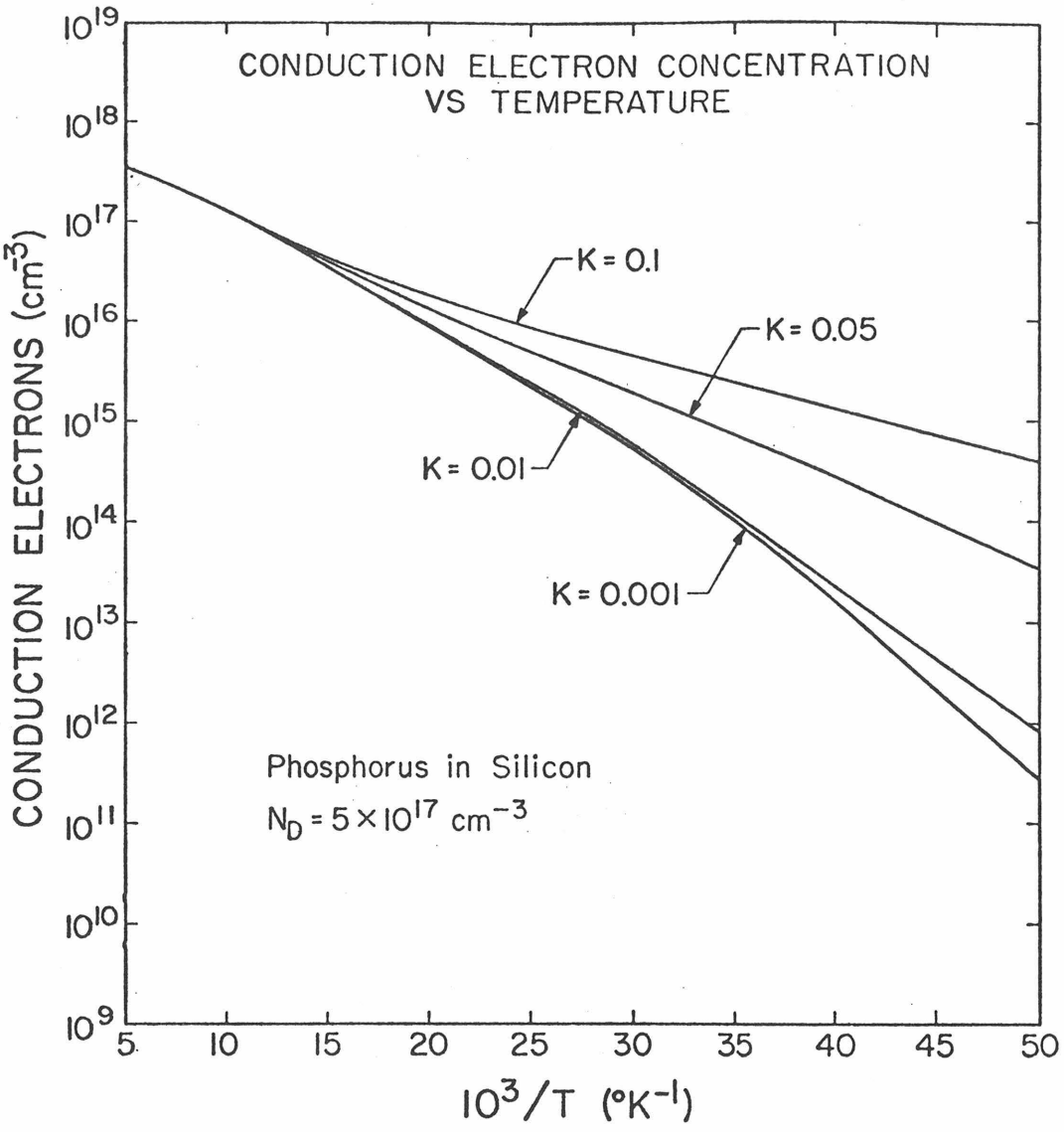

Fig. 3 The conduction electron concentration versus reciprocal temperature for different compensation ratios. The phosphorus concentration is $5 \times 10^{17} cm^{-3}$.

Table II. Values for ΔE_c, B, and σ for different compensation ratios and temperatures. The donor concentration is $5 \times 10^{17} cm^{-3}$.

N_A and N_D (cm^{-3})	K $\left(\frac{N_A}{N_D}\right)$	T (°K)	n (cm^{-3})	ΔE_c (meV)	B (meV)	σ (meV)
$N_A = 2.5 \times 10^{15}$	0.5%	25	1.52×10^{13}	1.93	19.3	3.79
$N_D = 5 \times 10^{17}$		200	3.73×10^{17}	11.3	19.3	13.6
$N_A = 5 \times 10^{16}$	10%	25	1.44×10^{15}	5.83	19.3	10.43
$N_D = 5 \times 10^{17}$		200	3.42×10^{17}	12.1	19.3	15.0

increased. Therefore, the increase of compensation ratio leads to decrease of activation energy.

These results may be compared with the experimental results of Penin et al[16] and the thorough experimental study of Swartz.[17]

The experimental results of Penin et al[16] indicate that the impurity-to-band activation energy depends upon the compensating impurity concentration and decreases as compensating impurity concentrations in Si increase. Thus the result of our calculation is in qualitative agreement with Penin's experimental result.

Swartz's[17] results of Hall measurements on Si samples doped with P, As, and Sb provide a rather rigorous check of the theory. Because of a lack of any information about what is the correct value of the Hall coefficient required to convert Hall coefficients to conduction electron concentrations, we take it to be the value appropriate to account phonon scattering, $3\pi/8$. The experimental result for conduction electron concentrations for P in Si along with calculated electron concentrations are plotted versus 1/T in Fig. 4. In this numerical calculation, the donor concentration N_D has been taken to be 1.6×10^{17} P/cm^3, a value which produced the best agreement between experiment and theory. The density of compensating centers was determined from the kink in the experimental n versus T^{-1} plot to be 10^{15}cm^{-3}. As we can see from Fig. 4, the agreement between the theory with all the corrections and experiment is very satisfactory. For comparison, we also plotted in Fig. 4 the calculated conduction electron concentration for a system with fixed activation energy of 44 meV and all the same donor and acceptor concentration. From Fig. 4 we notice that at low temperatures the decrease of activation energy produces a significant increase in the

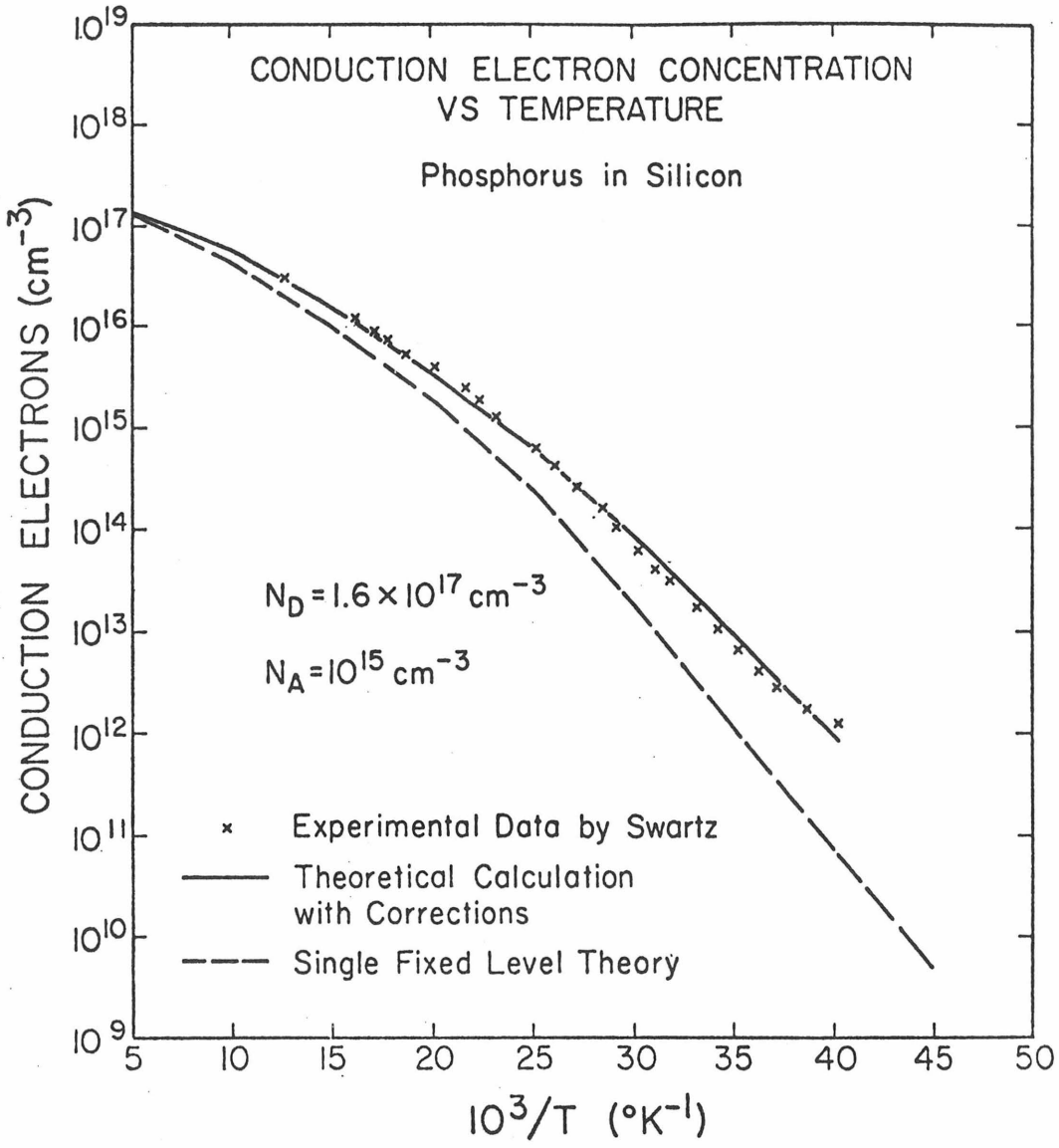

Fig. 4 The experimental and calculated conduction electron concentrations versus reciprocal temperature for phosphorus in silicon. The calculated results for a single fixed level theory is included for comparison.

conduction electron concentration

To compare our calculation with Swartz's experimental results on other dopants, we plotted the calculated electron concentrations versus 1/T along with experimental results for Si doped with Sb and As in Fig. 5 and Fig. 6, respectively. In these calculations, the ionization energies have been taken to be 39 meV for very low density of Sb in Si and 49 meV for very low density of As in Si. In Fig. 5, the compensating acceptor concentrations have been determined in the same way as in the case of P in Si. The Sb concentrations have been chosen to give best agreement between theory and experiment. As we can see, the agreement is quite good for case of Sb in Si. In Fig. 6, we compare the experimental and theoretical results for As in Si. The theoretical calculations for the case $N_D = 4 \times 10^{17} cm^{-3}$ and $N_A = 10^{15} cm^{-3}$, and $N_D = 7 \times 10^{17} cm^{-3}$ and $N_A = 10^{15} cm^{-3}$ are in satisfactory agreement with the experimental results. However for samples doped with more than 10^{18} As/cm^3, we can only obtain qualitative agreement between theory and experiment.

VI. DISCUSSION AND CONCLUSIONS

The self-consistent calculation by Lehman and James[4] essentially include two effects: the lowering of the conduction band edge and the shift of the ground state level of the donor due to conduction electron screening. While their results are successful at accounting for experimental results at small donor concentrations and with small amounts of compensation, they are inadequate at higher impurity concentrations. In this paper

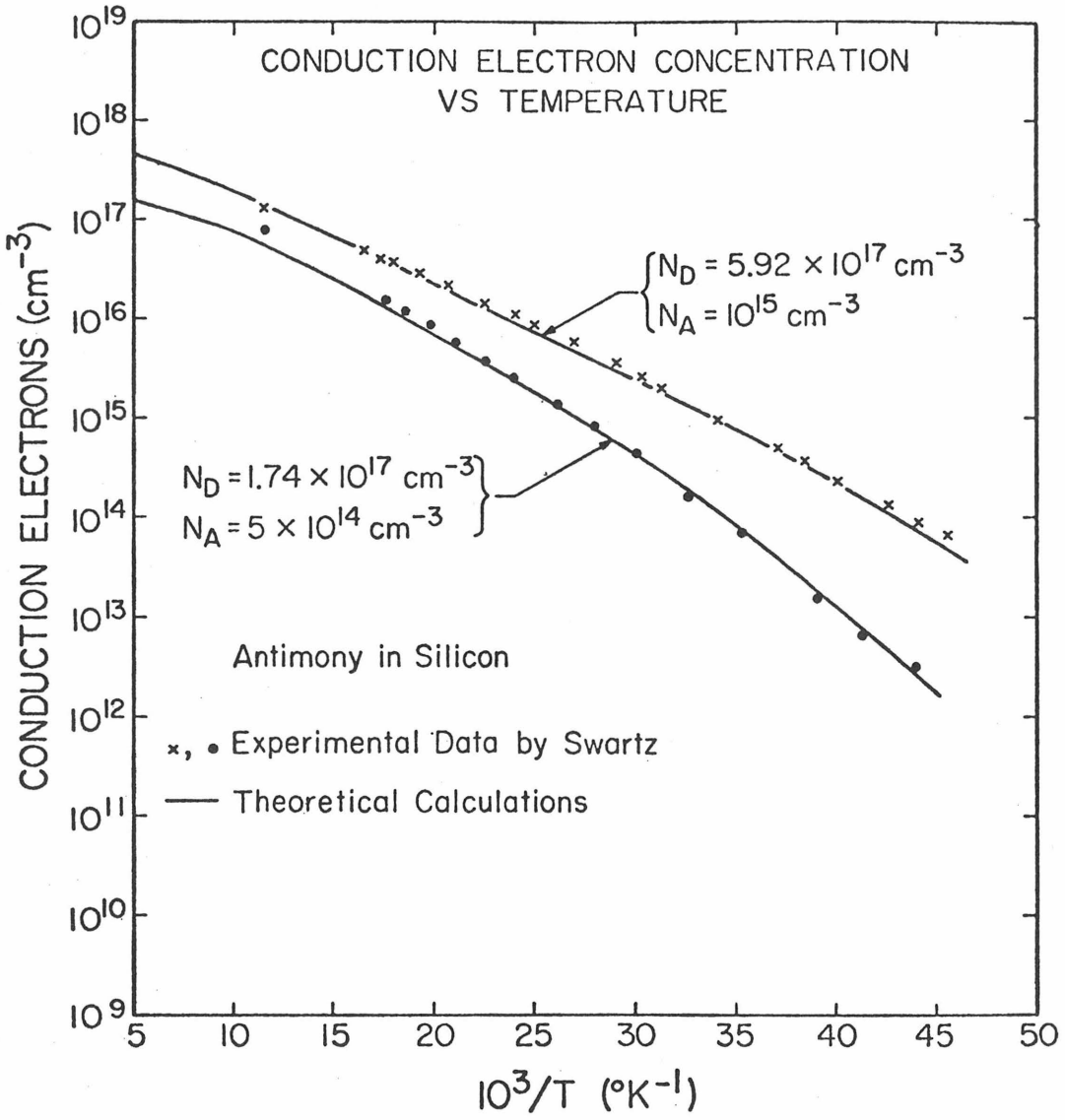

Fig. 5 The experimental and calculated conduction electron concentrations versus reciprocal temperature for antimony in silicon.

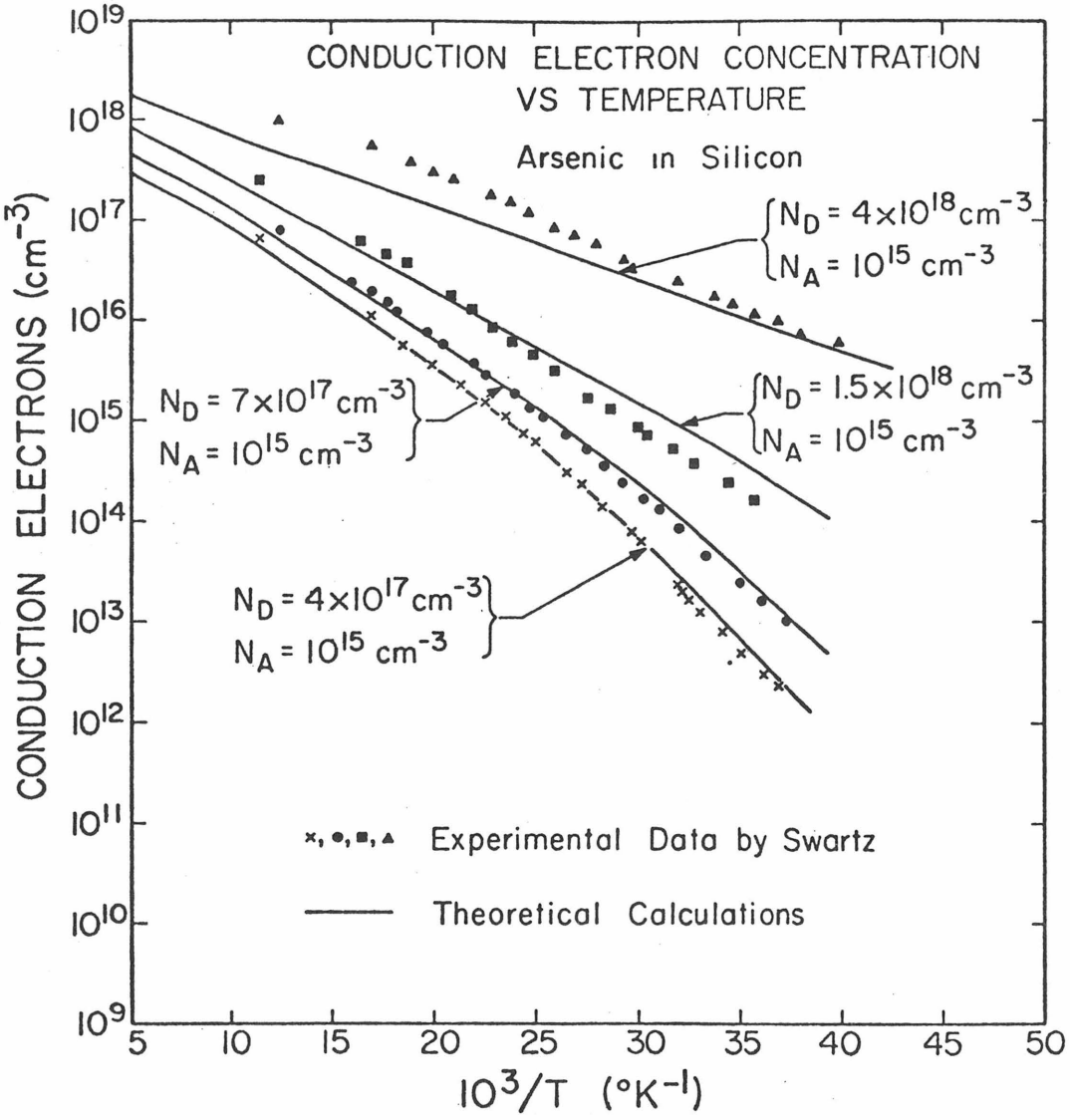

Fig. 6 The experimental and calculated conduction electron concentrations versus reciprocal temperature for arsenic in silicon.

we have introduced two additional effects: the broadening of the impurity level due to a finite energy transfer integral between wavefunctions localized on neighboring sites and potential fluctuations, and the tail on the conduction band edge due to potential fluctuations. The addition of these effects were shown to bring about good agreement between experimental results and theory for moderate impurity concentrations. However, at even higher impurity concentrations ($N_D \gtrsim 4 \times 10^{18} cm^{-3}$) even these effects are incapable of explaining the experimental results. This suggests that the problem is more complicated in this range.

The importance of broadening of the impurity level and band tailing on the conduction band edge found in these calculations suggest that one may not think of the single activation energy for $N_D \gtrsim 10^{17} cm^{-3}$. Interpretation of the Arrehnus plot in terms of single activation energy would then require that a temperature dependent activation energy.

APPENDIX

We first calculated the potential due to donor atom, i.e. one ionized donor plus one trapped electron. In response to the potential of the donor atom, the conduction electron readjust themselves to screen the potential. We calculated the screening conduction electron distribution by using linearized Hartree approximation. Since the potential due to the screening conduction electrons is small, we then calculated the donor ground state level shift by using first order perturbation theory.

To obtain the potential due to the donor ion and trapped electron, we assume that the trapped donor electron has `1s ground state wavefunction with Slater coefficient , i.e.

$$\phi_o(\vec{r}) = \sqrt{\frac{\xi^3}{\pi}}\, e^{-\xi r} \quad , \qquad \text{(A-1)}$$

where $r = |\vec{r}|$. The potential of the neutral donor atom is thus equal to

$$V_n(\vec{r}) = \frac{q^2}{4\pi\varepsilon\varepsilon_o}\left[\frac{1}{r} + \xi\right] e^{-2\xi r} \quad . \qquad \text{(A-2)}$$

Subject to the neutral donor atom potential, $V_n(\vec{r})$, the conduction electrons readjust themselves and try to screen the potential. Under Hartree approximation and linear response theory, the screened potential is given by

$$V_{nc}(\vec{r}) = \frac{1}{(2\pi)^3}\int \tilde{V}_{nc}(\vec{K})\, e^{i\vec{K}\cdot\vec{r}}\, d^3K \quad , \qquad \text{(A-3)}$$

with

$$\tilde{V}_{nc}(\vec{K}) = \frac{\tilde{V}_n(\vec{K})}{1 + \tilde{V}_n(\vec{K}) \frac{\varepsilon\varepsilon_0}{q\lambda_e^2}} \quad , \qquad \text{(A-4)}$$

where λ_e is conduction electron screening length and $V_n(\vec{K})$ is the Fourier transformation of $V_n(\vec{\gamma})$, i.e.

$$\tilde{V}_n(\vec{K}) \equiv \int V_n(\vec{\gamma})\, e^{-i\vec{K}\cdot\vec{\gamma}}\, d^3\gamma$$

$$= \frac{q^2}{\varepsilon\varepsilon_0} \left[\frac{K^2 + 8\xi^2}{(K^2 + 4\xi^2)^2} \right] \quad , \qquad \text{(A-5)}$$

with $K = |\vec{K}|$. In view of (A-4) and (A-5), the integral can be carried out and, for $\xi\lambda_e > \frac{1}{4}$, leads to

$$V_{nc}(\vec{\gamma}) = \frac{2q^2}{\pi\varepsilon\varepsilon_0\gamma}\, \lambda_e^2\xi^2\, f\, e^{-2g\xi\gamma}\, \sin\left[2\tan^{-1}f + 2h\xi\gamma\right] \quad , \qquad \text{(A-6)}$$

with

$$f = \frac{1}{\sqrt{16\xi^2\lambda_e^2 - 1}} \quad ,$$

$$g = \left[\frac{1}{2} + \frac{1}{16\xi^2\lambda_e^2} + \frac{1}{2}\left(1 + \frac{1}{2\xi^2\lambda_e^2}\right)^{1/2} \right]^{1/2} \quad ,$$

and

$$h = \left[\frac{1}{2}\left(1 + \frac{1}{2\xi^2\lambda_e^2}\right)^{1/2} - \frac{1}{2} - \frac{1}{16\xi^2\lambda_e^2} \right]^{1/2} \quad .$$

For the case we are interested in the conduction electron screening length is larger than the trapped electron average radius $1/\xi$, i.e. $\lambda_e\xi > 1$. The

series expansion of $V_{nc}(\gamma)$ to the first order of $\frac{1}{\xi\lambda_e}$ gives

$$V_{nc}(\vec{\gamma}) \equiv \frac{q^2\xi\lambda_e}{2\pi\varepsilon\varepsilon_o\gamma}\ e^{-2\xi\gamma}\ \sin\left(\frac{1+\xi\gamma}{2\xi\lambda_e}\right) \quad , \qquad \text{(A-7)}$$

with the residual terms of the order of $\left(\frac{1}{\xi\lambda_e}\right)^2$. Therefore the potential due to donor ion and screening electrons only is given by

$$\begin{aligned} V_c(\vec{\gamma}) &= V_{nc}(\vec{\gamma}) + \frac{q^2}{4\pi\varepsilon\varepsilon_o}\left[\frac{1}{\gamma} - \left(\frac{1}{\gamma}+\xi\right)e^{-2\xi\gamma}\right] \\ &= \frac{q^2}{4\pi\varepsilon\varepsilon_o\gamma} - \frac{q^2e^{-2\xi\gamma}}{4\pi\varepsilon\varepsilon_o}\left[\frac{1}{\gamma}+\xi-\frac{2\xi\lambda_e}{\gamma}\sin\left(\frac{1+\xi\gamma}{\lambda_e\xi}\right)\right] \end{aligned} \qquad \text{(A-8)}$$

The potential seen by the trapped electron is different from Coulomb potential by

$$V'(\vec{\gamma}) = -\frac{q^2e^{-2\xi\gamma}}{4\pi\varepsilon\varepsilon_o}\left[\frac{1}{\gamma}+\xi-\frac{2\xi\lambda_e}{\gamma}\sin\left(\frac{1+\xi\gamma}{2\ \xi\lambda_e}\right)\right] \quad , \qquad \text{(A-9)}$$

and the ground state energy shift in first order perturbation theory is given by

$$\begin{aligned} \Delta E_B &= V_{oo}' \equiv \langle\phi_o\ |V'|\phi_o\rangle \\ &= \frac{q^2\xi}{4\pi\varepsilon\varepsilon_o}\left\{\frac{3}{8} - \frac{2\xi\lambda_e\ \sin\left[\frac{1}{2\xi\lambda_e}+2\ \tan^{-1}\frac{1}{8\xi\lambda_e}\right]}{4+\frac{1}{16\xi^2\lambda_e^{\ 2}}}\right\} \end{aligned} \qquad \text{(A-10)}$$

REFERENCES

1. G. L. Pearson and J. Bardeen, Phys. Rev. 75, 865 (1949).
2. G. W. Castellan and F. Seitz, Semiconducting Materials (Butterworths, London, 1951), p. 8.
3. L. Pincherle, Proc. Phys. Soc. (London) A64, 663 (1951).
4. G. W. Lehman and H. M. James, Phys. Rev. 100, 1698 (1955).
5. P. P. Debye and E. M. Conwell, Phys. Rev. 93 , 693 (1954).
6. E. O. Kane, Phys. Rev. 131, 79 (1963).
7. T. N. Morgan, Phys. Rev. 139, A343 (1965).
8. E. K. Kudinov and S. T. Pavlov, JETP 15, 585 (1962).
9. V. L. Bonch-Brayevich, The Electronic Theory of Heavily Doped Semiconductors.
10. V. B. Glasko and A. G. Mirmov, Sov. Phys. Solid State 4, 241 (1962).
11. F. J. Blatt, "Physics of Electronic Conduction in Solids," (McGraw-Hill Book Company, New York, 1968), p. 178.
12. E. G. S. Paige, Progress in Semiconductors 8 (ed. by Gibson and Burgess John Wiley and Sons, Inc., New York, 1964) p. 77.
13. J. M. Ziman, "Principles of the Theory of Solids" (Cambridge University Press, London, 1964) p. 82.
14. W. Kohn, Solid State Phys. Vol. 5 (Academic Press, New York, 1957) p.257.
15. S. M. Sze, "Physics of Semiconductor Device" (John Wiley and Sons, Inc., New York, 1969) p. 30.
16. N. A. Penin, B. G. Zhurkin and B. A. Volkov, Soviet Phys. Solid State 7, 2580 (1966).
17. G. A. Swartz, J. Phys. Chem. Solids 12, 245 (1960).

PART FOUR

INVESTIGATION OF TELLURIUM IMPLANTED SILICON

Generally, deep level impurities have low solid solubilities in semiconductors. Therefore, by conventional doping techniques such as thermal diffusion, it is difficult to heavily dope the semiconductors with deep level impurities. Ion implantation,[1] however, offers the possibility for introducing high concentrations of deep level dopants in silicon. MeV He channeling studies have been made of the lattice location of a wide variety of dopant species in Si.[2] Of these dopant species, tellurium would appear to be attractive for evaluation of electrical properties because of its high substitutional fraction[3] and deep level.[4]

When Te is implanted at low doses ($\lesssim 4 \times 10^{12}$ cm^{-2}), it acts as an n-type dopant with an activation energy of 140 meV.[5] However, samples implanted with high doses (typically 10^{14} - 10^{15} cm^{-2}) exhibit a somewhat puzzling behavior; the number of conduction electrons has a temperature activation energy which is about zero; and the measured number of conduction electrons is some two orders of magnitude smaller than number of implanted Te.[6] From conventional semiconductor theory,[7] one would anticipate that for heavily doped semiconductors which have a zero activation energy, the number of conduction electrons would be nearly equal to the number of substitutional impurities. In this work, we pursue the apparent contradiction between a zero activation energy and the small number of conduction electrons as compared to the number of substitutional Te dopants.

We have investigated several experimental aspects that could influence the measured electrical activity: (i) the non-uniform depth distribution of the implanted Te, (ii) the influence of radiation damage, and (iii) formation of substitutional clusters of Te. Previous Hall effect measurements on high dose Te implanted samples[6] were made without use of layer-removal techniques.[8] The measured number of conduction electrons/cm^2, N_s, is usually smaller than the actual number present due to the mobility weighting factor. This weighting effect can be overcome by differential measurements which combine Hall effect and resistivity measurements with layer removal technique. This differential technique coupled with measurements as a function of temperature has been found to give activation energies consistent with those for bulk doped samples for silicon implanted with indium and Te at low concentrations.[5,10] In this work we have used differential techniques to obtain the temperature dependence of the carrier concentration for substitutional Te concentration between 10^{17} - $10^{20}/cm^3$.

For implanted samples, residual radiation damage can remain after high temperature anneal. The radiation defects may act as compensation centers and thus reduce the number of conduction electrons. To investigate the effect of implantation radiation damage, we performed electrical measurements on low dose (10^{12} to $10^{13}/cm^2$) phosphorus implanted Si samples with and without pre-damage introduced by a higher dose ($10^{15}/cm^2$) of Si ions. If the radiation damage is responsible for the

reduction in the number of electrons/cm^2 for the Te case, we would expect that the electrical activity of phosphorus implanted samples with pre-damage would be much less than the electrical activity of phosphorus implanted samples without pre-damage.

In arsenic diffused samples, it has been found[11] that the electrical activity is reduced by long heat treatment at temperatures of 500-970°C. The electrical activity could be increased by heating at higher temperatures (approx. 1100°C) and then quenching. The reduction of electrical activity was attributed to the formation of As clusters which could be dissociated during high temperature processing. Similar effects may play a role in high dose Te implanted samples where the concentration of Te (10^{19} to $10^{20}/cm^3$) can be orders of magnitude above the reported[4] thermal equilibrium solid solubility of $10^{17}/cm^3$. To investigate the influence of cluster formation we employed high temperature heat treatment followed by quenching for some samples. In analogy with As results, this treatment should lead to high electrical activity if formation of Te clusters were responsible for the relatively low electron concentrations.

From a theoretical approach, we used the model proposed by Lee and McGill[12] to treat the decrease of activation energy with increasing impurity concentrations. In this case, we calculated the conduction electron concentrations as a function of temperature for different Te concentrations to determine whether there is contradiction between the almost zero activation energy and the reduction in conduction electron concentrations.

This paper is organized in the following way. Section II contains the experiment and analysis procedures. In Section III we describe the procedure of calculating electron concentrations as a function of temperature. In Section IV, we present the experimental results and compare them with theoretical calculations.

II. EXPERIMENTAL AND ANALYSIS PROCEDURES

2.1 Sample Preparation

Implantations of tellurium were made at energies between 100 and 220 keV in etch-polished slices of float-zoned 10 and 2000 Ω-cm p-type silicon. The projected ranges for 100 and 220 keV tellurium implantation in silicon are 456 Å and 870 Å, respectively.[13] Ion doses ranged between $4 \times 10^{12} cm^{-2}$ to $1.4 \times 10^{15} cm^{-2}$. Ion implantations of phosphorus were made at energies between 7 and 190 keV and ion doses between $3 \times 10^{12} cm^{-2}$ and $3 \times 10^{13} cm^{-2}$. The projected range of silicon implantation for pre-damage was deeper than those of phosphorus implantations; the silicon dose was $10^{15} cm^{-2}$. All the substrates were at room temperature.

Hall effect and sheet resistivity measurements were made using the van der Pauw configuration.[14] The van der Pauw pattern was defined on the implanted surface by masking with photoresist followed by mesa etching. The mesa structure in combination with the p-n junction between the implanted layer and substrate isolated the region of interest.

After the van der Pauw patterns were put on the implanted specimens, they were placed in a quartz tube furnace with flowing N_2 to anneal out the radiation damage. The P-implanted samples have been annealed to 850°C for 15 to 30 minutes. For Te implanted samples, isothermal anneal cycles have been performed to determine the anneal temperature where the number

of electrons/cm^2 was near the maximum value. The anneal behavior of several samples were shown in Fig. 1, in which the measured number of electrons/cm^2 and the electron mobility were plotted as a function of anneal temperature. As found previously,[15] the number of electrons/cm^2 is much lower than the number of Te/cm^2. For the highest dose implant shown there is a factor of 60 difference between the two values. As shown in Fig. 1, the number of electrons/cm^2 and the electron mobility stayed essentially at the same value over the anneal temperature between 800 and 1000°C. Therefore, anneal temperatures between 800 and 1000°C for 15 to 30 minutes have been chosen for all the samples.

MeV He ion backscattering and channeling measurements were made on several annealed Te implanted samples to confirm the previous results which indicated high (60%) substitutional percent of Te atoms.[3] The highest substitutional percent we obtained was 80% for a sample implanted with 1.4×10^{14} Te/cm^2 and the lowest was 30% for a dose of 1.4×10^{15} Te/cm^2. As pointed out previously, these results indicate that the low electrical activity of Te implanted layers cannot be due entirely to non-substitutional Te.

2.2 Layer Removal Techniques

Layer removal was accomplished by using oxide layer stripping techniques. In practice, a layer of silicon dioxide was anodically grown on the sample and then removed by etching. A vinyl mask was used to define the area of the anodic oxide on the sample which was then securely clamped below a hole at the bottom of a teflon beaker. The anodic solution contained in the beaker was made from 97% N-methylacetamide, 2% triply distilled water and 1% potassium nitrate by weight. A constant current

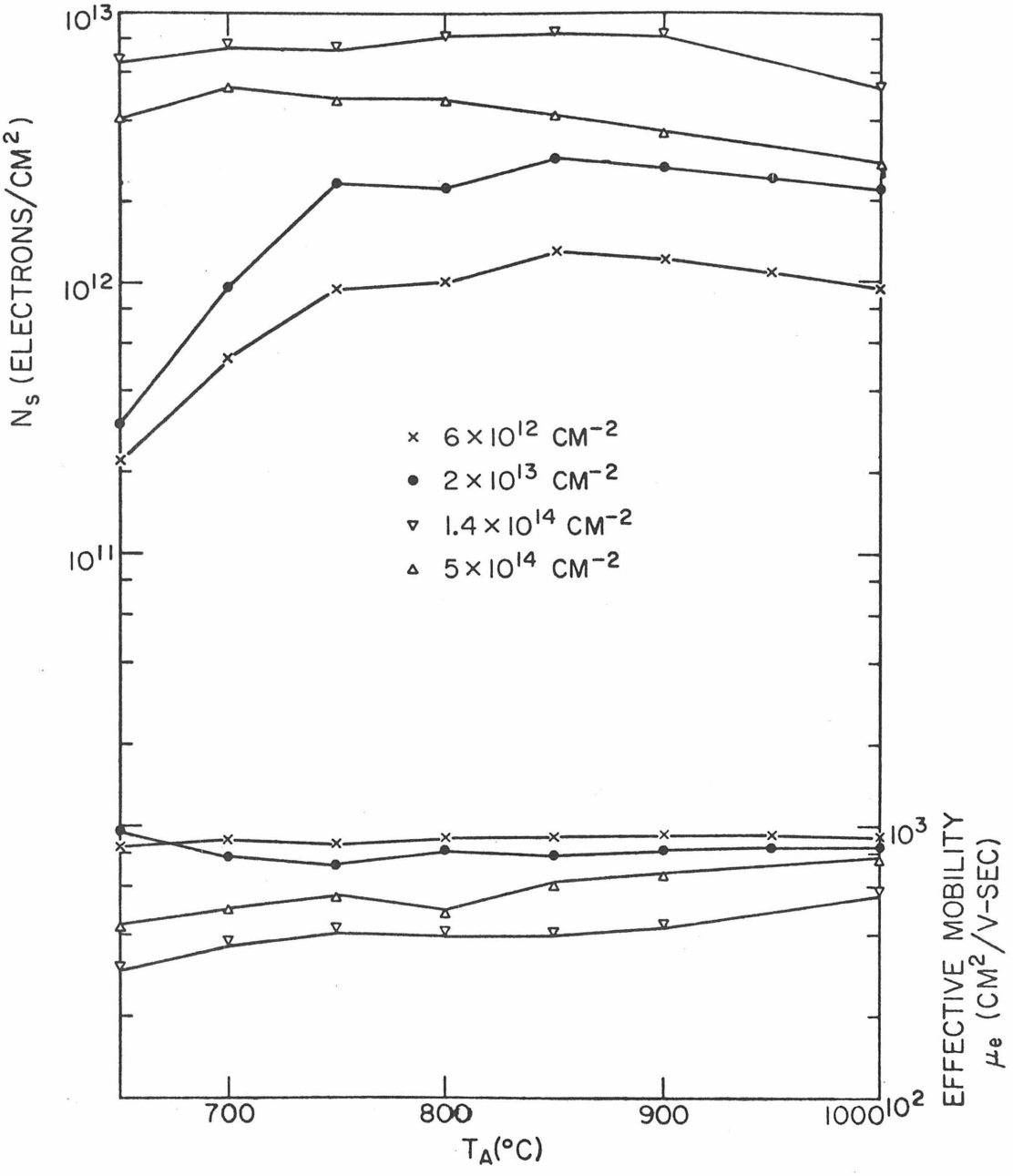

Figure 1. Anneal behavior of the surface electron concentration N_s and the effective mobility μ_e for silicon implanted at room temperature with 220 KeV Te ions.

density of 9 ma/cm^2 in the presence of high intensity light was used during the process of anodization.

Ellipsometry measurements were made to determine the thickness-voltage dependence. The oxide thicknesses were found to be reproducible within 5%. The oxide layer was stripped with concentrated hydrofluoric acid (HF). The thickness of removed silicon layer was assumed to be 43% of the thickness of oxide layer.

2.3 Electrical Measurements

Hall effect and sheet resistivity were measured as a function of temperature. The desired temperature was maintained through heat exchange in a gas flow liquid nitrogen cryostat. The platinum sensor and controller held temperatures to within $\pm$ 0.2°K. A magnetic field of 4 K Gauss has been employed for Hall effect measurements. Measurements were performed using pressure contact to the implanted layers.

As a result of Hall effect and sheet resistivity measurement, the number of electrical carriers/cm^2, N_s, and sheet resistivity ρ_s can be obtained if we assume that the Hall mobility is equal to drift mobility. This assumption is valid for heavily doped semiconductor samples.[16] For low dose samples, this assumption may give rise to, at most, a factor of two error. By combining layer removal technique with Hall effect and sheet resistivity measurement we can obtain the average carrier concentration and resistivity of the removed thin layer through the relationship[8]

$$n_i = \frac{\left[\left(\frac{1}{\rho_s}\right)_i - \left(\frac{1}{\rho_s}\right)_{i+1}\right]^2}{d_i\left[\left(\frac{1}{\rho_s^2 N_s}\right)_i - \left(\frac{1}{\rho_s N_s}\right)_{i+1}\right]} \quad , \qquad \text{(II.1)}$$

$$\rho_i = d_i\left[\left(\frac{1}{\rho_s}\right)_i - \left(\frac{1}{\rho_s}\right)_{i+1}\right] \quad . \qquad \text{(II.2)}$$

Where $(N_s)_{i+1}$ and $(\rho_s)_{i+1}$ are measured carriers/cm^2 and sheet resistivity after the removal of the i^{th} layer; d_i is the thickness of the removed i^{th} layer.

2.4 Quenching

To perform the quenching experiments, we set the furnace at an upright position so that the samples could move freely in the vertical direction. The samples were placed in a quartz basket with several holes at the bottom. At the end of the annealing time period, the quartz basket and samples were dropped within 0.2 sec into a beaker containing de-ionized water. The samples were cycled through a series of heat treatments which involved anneal at 1000°C followed by a quench and then anneal at 850°C without a quench. Electrical measurements were made before and after each anneal.

III. THEORY OF ACTIVATION ENERGY VARIATION

The ratio of conduction electron concentration to the impurity concentration at various temperatures depends upon the impurity activation energy. Hence, any variation of impurity activation energy would cause a change of the values of the electron-to-impurity-concentration ratio. It has been reported that the impurity-to-band activation energy decreases

at high impurity concentration in semiconductors.[17] Recently, Lee and McGill[12] have worked out a theory for the variation of activation energy with impurity concentrations. They pointed out that the donor activation energy decreases because of both donor level shifting and donor level broadening.

To illustrate the model of their theory, the conduction band density-of-states, $N_c(E)$, and the donor level density-of-states, $\rho_i(E)$, are plotted in Fig. 2 for the cases of both low donor concentrations and high donor concentrations. For low donor concentration case, the conduction band edge and the discrete donor level are well defined. The donor activation energy is unique and equal to E_D. For high donor concentration case, in addition to the strict shift of conduction band edge toward the donor level, ΔE_c, the broadening of the donor states and the tail of the conduction band edge also contribute to the decrease of donor activation energy. Due to the donor state broadening effect, some impurity states shift upward toward the conduction band edge and some shift downward away from conduction band edge, as shown in Fig. 2. The upward shifted states contribute partly to the decrease of the activation energy and the downward shifted states are mostly occupied by electrons and thus correspond to the non-ionized portion of Te impurities. The donor activation energy is not uniquely defined and thus varies as a function of temperature. Further, even though the apparent activation can decrease to values near zero, the donor atoms are not all ionized.

Using this physical model, we calculated the conduction electron concentration as follows: The conduction electron concentration n is

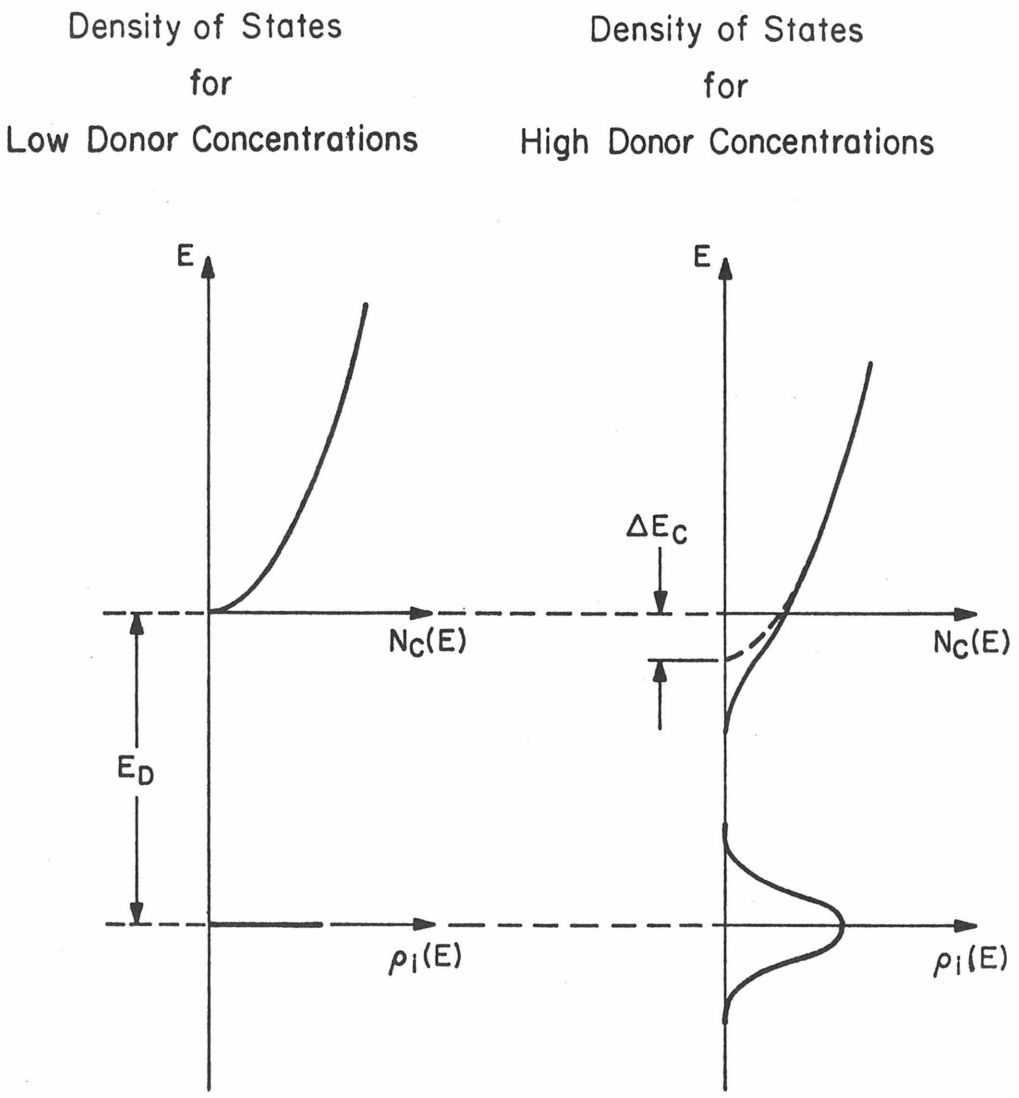

Figure 2. The physical model for the decrease of activation energy with increasing impurity concentrations.

given by the standard expression

$$n = \int_{-\infty}^{\infty} \frac{N_c(E - \Delta E_c)}{1 + \exp\left(\frac{E-E_f}{K_B T}\right)} \, dE \quad , \qquad \text{(III.1)}$$

where E_f is Fermi energy, K_B is ~~Blotzmann~~ Boltzmann constant, T is absolute temperature, $N_c(E)$ is conduction band density of states and ΔE_c is the lowering of conduction band edge due to attraction between conduction electrons and ionized donors. Because of conduction band edge smearing due to potential fluctuation, the shape of $N_c(E)$ is different from that of intrinsic Si. The expressions for $N_c(E)$ and ΔE_c are given in Appendix. Similarly, the concentration of ionized donors is defined as

$$N_D^+ = \int_{-\infty}^{\infty} \frac{\rho_i(E-E_D)}{1 + g \exp\left(\frac{E_f-E}{K_B T}\right)} \, dE \quad , \qquad \text{(III.2)}$$

where g is the degeneracy factor for the donor ground state, $\rho_i(E)$ is the donor level density of states and $(-E_D)$ is the donor ionization energy at low donor concentrations. The factor $\rho_i(E)$ depends upon the effects of donor level broadening due to donor electron wavefunction overlapping and the effect of donor state spreading due to potential fluctuation. The expression for $\rho_i(E)$ is also given in Appendix. For donors, such as P in Si, the hydrogen model is suitable to describe the donor states and thus g is assumed to be equal to 2. For donors, such as Te in Si, the helium model seems to be appropriate to describe the donor states and thus g is assumed to be equal to 1/2.[18]

With the presence of compensating acceptor concentration N_A, charge neutrality leads to

$$n + N_A = N_D^+ \quad , \qquad \text{(III.3)}$$

which determines the Fermi level E_f and, in turn, determines the conducting electron concentration n from Eq. (III.1). The presence of compensation centers not only reduces the number of electrons but also introduces additional broadening due to increased potential fluctuations.[12]

IV. RESULTS

For the purpose of investigating the influence of residual radiation damage on the electrical properties of implanted samples, we investigated the influence of damage caused by pre-implantation of Si ions. In Fig. 3 the measured numbers of electrons/cm^2, N_s, versus 1/T are given for two samples; one of the sample was phosphorus implanted to $3 \times 10^{13} cm^2$ with Si ion pre-damage and the other sample was phosphorus implanted to $3 \times 10^{12} cm^{-2}$ without pre-damage. For both of the samples, the numbers of electrons/cm^2 at room temperature were equal to two/thirds of phosphorus concentrations. Therefore, the Si ion pre-damage does not seem to result into significant reduction of number of conduction electrons at room temperature.

To investigate the effect of residual radiation damage in more detail, we used differential measurements to obtain the carrier concentration as a function of temperature. Therefore, in Fig. 3 the measured numbers of electrons/cm^2 versus 1/T are shown for both of the samples after a

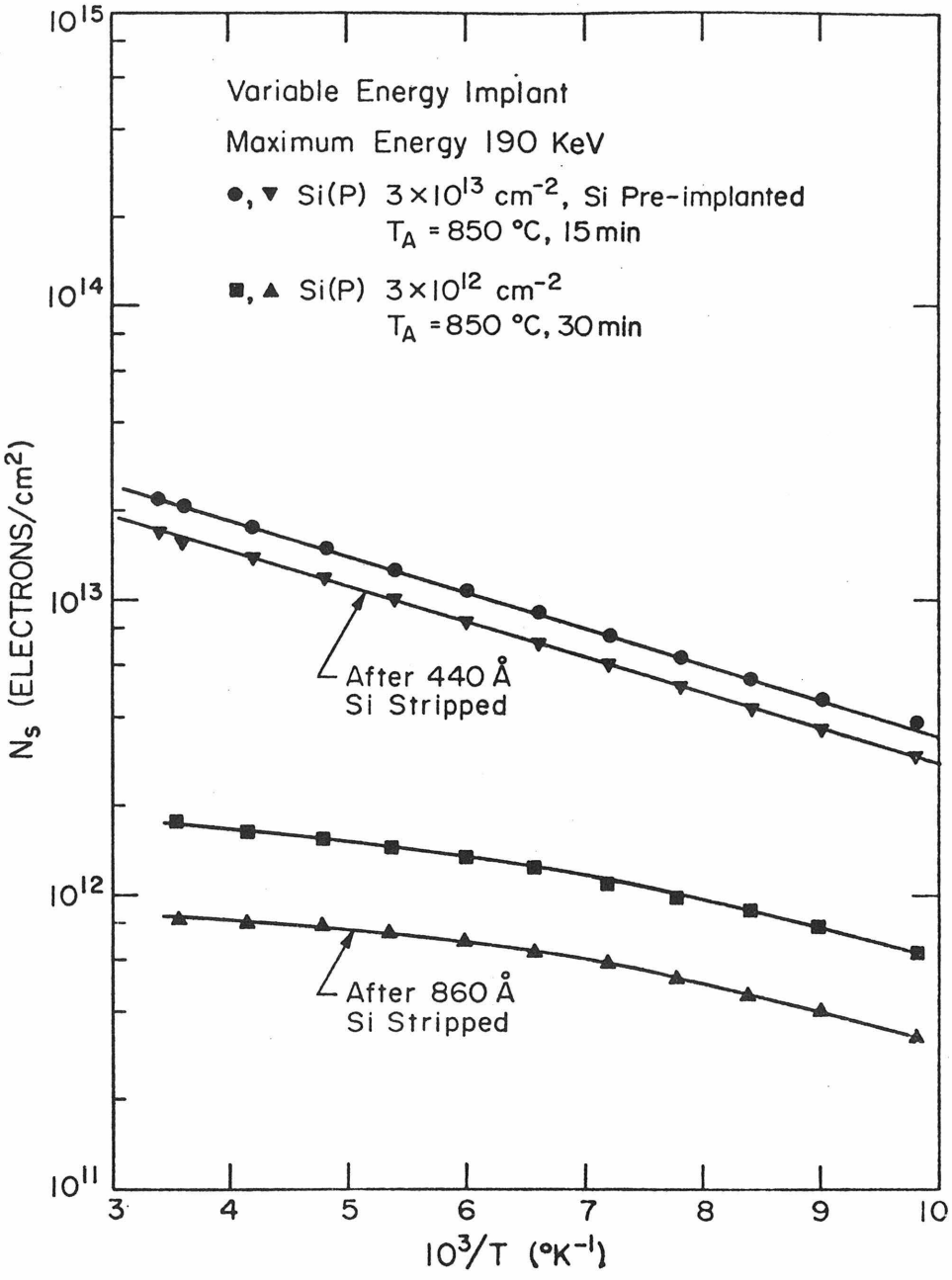

Figure 3. The surface electron concentration N_s versus reciprocal temperature for two P-implanted silicon samples before and after a thin layer was removed.

layer was removed. The results of the differential measurements are shown in Fig. 4 which gives the concentration of electrons/cm^3 versus 1/T. The conduction electron concentrations at room temperature are about $10^{18} cm^{-3}$ for sample implanted with phosphorus 3×10^{13} cm^{-2} and about 9×10^{16} cm^{-3} for sample implanted with phosphorus 3×10^{12} cm^{-2}. To compare the experimental results with theoretical calculations (see Appendix) we also plotted in Fig. 4 the calculated conduction electron concentrations as a function of 1/T. The donor concentrations N_D and the compensating acceptor concentration N_A were chosen to give best agreement between the theory and experiment. The numerical calculations with $N_D = 1.2 \times 10^{18}$ cm^{-3} and $N_A = 10^{15}$ cm^{-3} was in good agreement with the experimental results of sample implanted with phosphorus 3×10^{13} cm^{-2}. Similarly, the numerical calculation with $N_D = 9 \times 10^{16}$ cm^{-3} and $N_A = 10^{15}$ cm^{-3} was also in satisfactory agreement with the experimental results of sample implanted with phosphorus 3×10^{12} cm^{-2}. The concentrations of compensating centers N_A are two to three orders of magnitude below the phosphorus concentration. The good agreement between the theory and experiment on phosphorus implanted Si samples indicated that the effect of the residual radiation damage was negligible. Although this is not conclusive evidence for an absence of damage effects in the Te case, it does suggest that radiation damage is not the major factor responsible for the low activity.

We investigated the electrical properties of Te implanted samples by performing Hall effect and resistivity measurements. From the sign of the Hall voltage, we deduced that implanted Te has donor behavior in Si, in agreement with the result of Te doped bulk Si samples.[4]

The anneal of Te implanted samples to 1000°C and rapid quench to

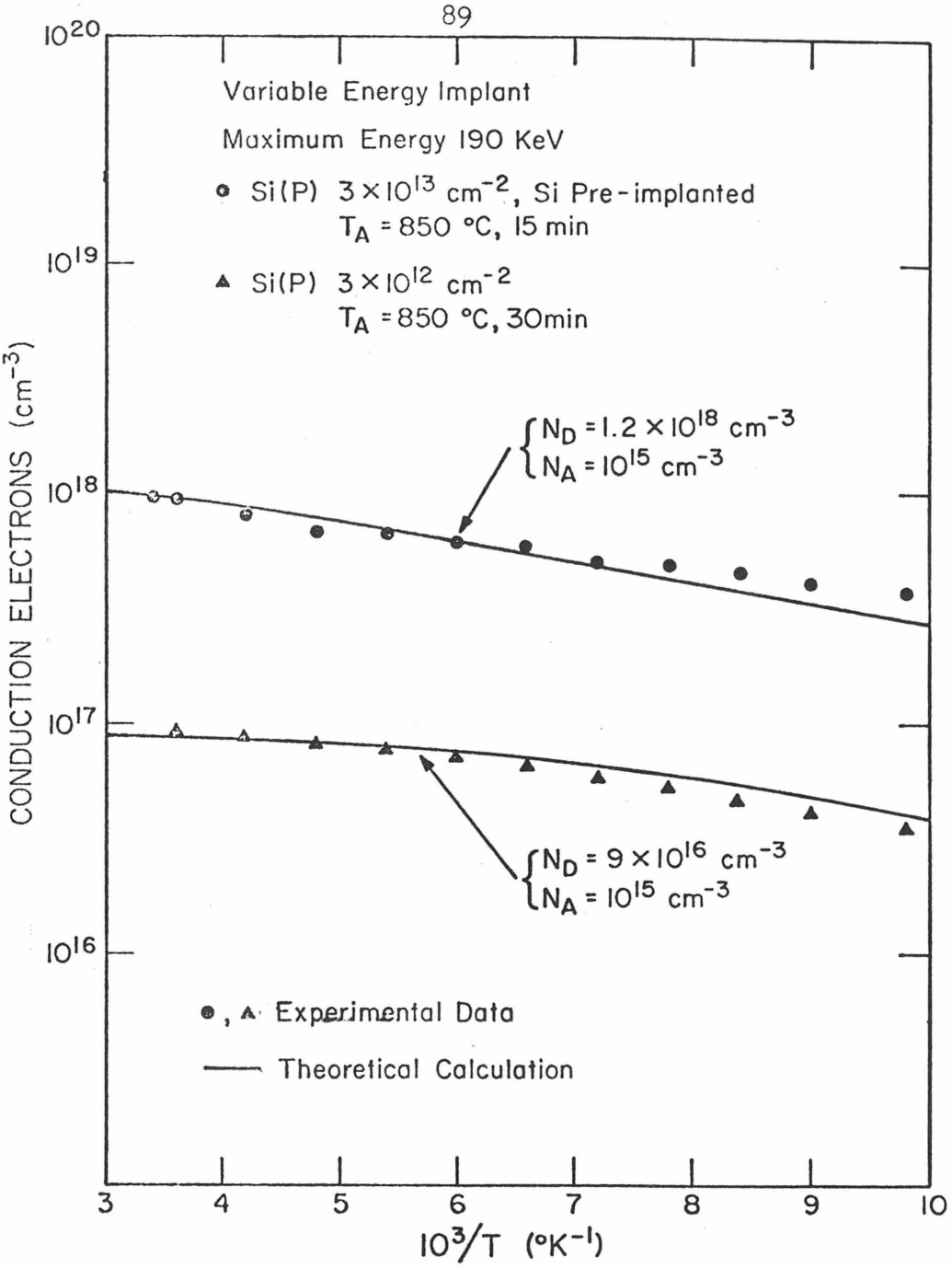

Figure 4. The conduction electron concentrations of differential measurements versus reciprocal temperature for P-implanted silicon samples. The calculated conduction electron concentrations versus reciprocal temperature for P in silicon are shown for comparison.

room temperature did not give significant increase of conduction electrons/cm^2. As discussed in Section 2.4, samples were processed through several quench and no-quench cycles. The values of N_s changed by about 10% throughout the quenching steps, but no systematic trend was noticed. Therefore, we do not believe that the formation of Te substitutional clusters could account for the entire difference between the number of electrons/cm^2 and the number of implanted Te atoms. It is possible, of course, that a temperature of 1000°C is not sufficient to dissociate Te clusters or that faster quenching is required.

The measured numbers of conduction electrons/cm^2, N_s, versus 1/T for several Te implanted samples were plotted in Fig. 5. For these samples, the lowest dose is 4×10^{12} cm^{-2} and the highest dose is 1.4×10^{15} cm^{-2}. In Fig. 5, the slopes of log N_s versus 1/T decrease as the Te concentrations increase. This indicates qualitatively that the Te activation energy decreases as Te concentration increases. For the sample implanted with Te 1.4×10^{15} cm^{-2}, the activation energy is approximately equal to zero but the number of conduction electrons/cm^2 is about 2×10^{13} cm^{-2} which is almost two orders of magnitude less than the number of implanted Te atoms. The upward curvature in the data for the high dose sample caused by mobility weighting has been observed in other measurements on Te implanted samples.[6]

The results of the differential measurements for three of the samples are plotted versus 1/T in Fig. 6. The slope of the curve for the sample implanted with 4×10^{12} Te cm^{-2} yields an activation energy of 140 meV, which agrees with the result of Te doped bulk Si samples.[4] As also found in Fig. 5, the activation energy in Fig. 6 decreases with increasing

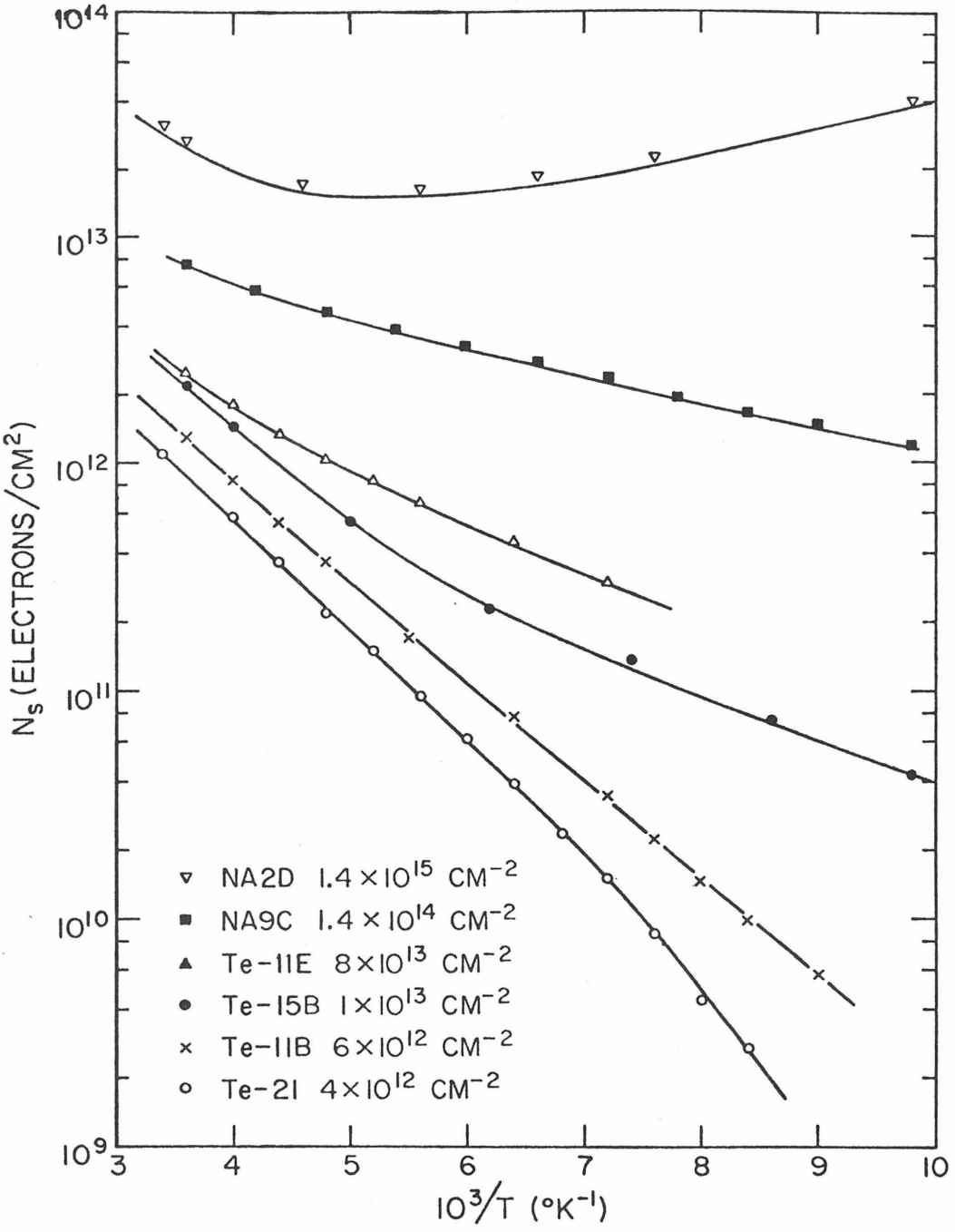

Figure 5. The surface electron concentration N_s versus reciprocal temperature for Te-implanted silicon samples.

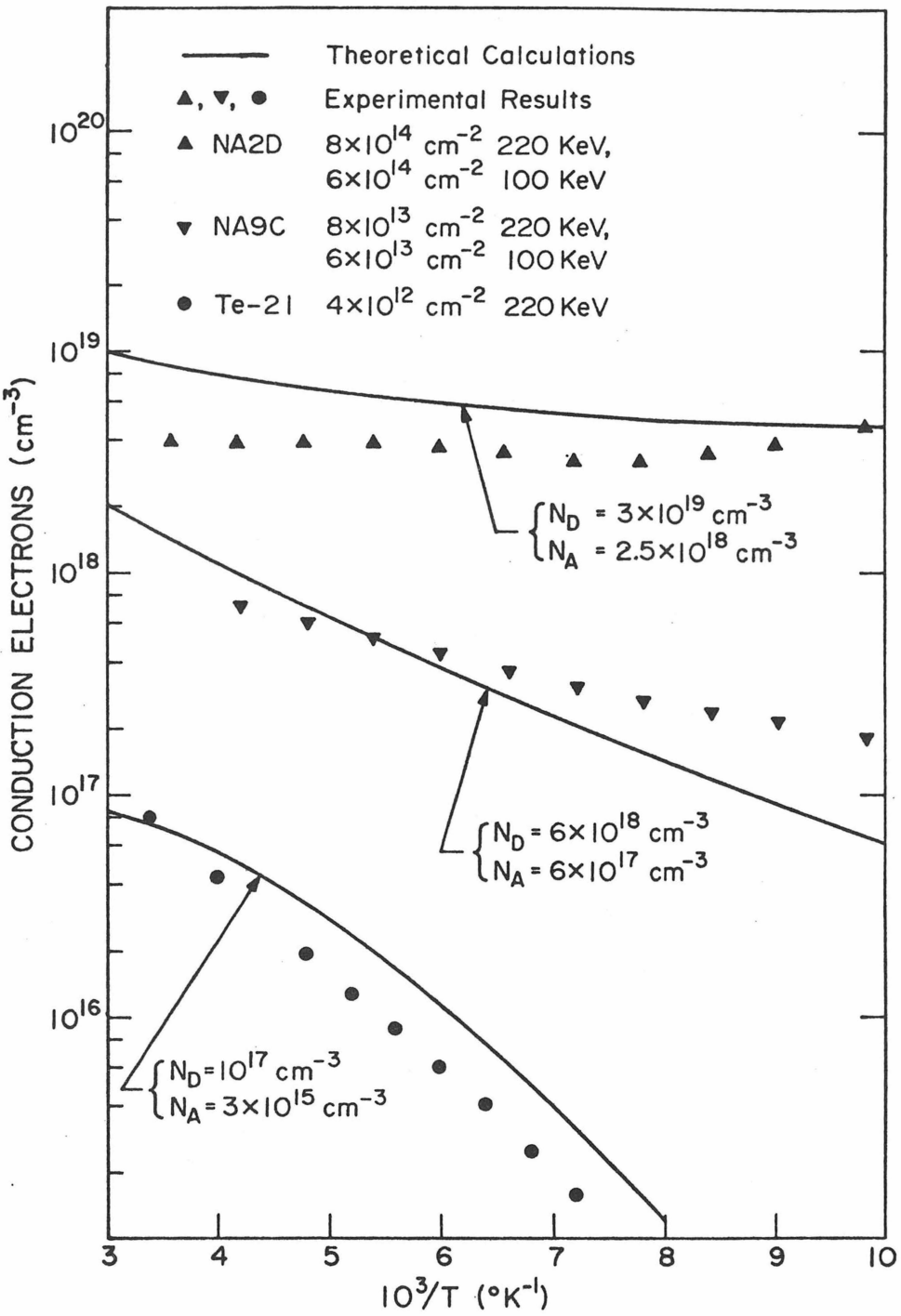

Figure 6. The conduction electron concentrations of differential measurements versus reciprocal temperature for Te-implanted silicon samples. The calculated conduction electron concentrations versus reciprocal temperature for Te in silicon are shown for comparison.

Te concentration. For the sample implanted with Te 1.4×10^{15} cm^{-2}, the measured conduction electron concentration does not vary between room temperature and 100°K.

To compare the experimental results with the results of the theoretical calculations, we also plotted in Fig. 6 the calculated conduction electron concentrations versus 1/T for different Te concentrations. The Te concentrations N_D and the compensating acceptor concentrations N_A shown in Fig. 6 were chosen to give best agreement with the experimental results. The numerical calculation with $N_D = 3 \times 10^{19}$ cm^{-3} and $N_A = 2.5 \times 10^{18}$ cm^{-3} indicated that the conduction electron concentrations varied very little over the temperature range between room temperature and 100°K. As we can see from Fig. 6 the experimental and the theoretical results have some similar behavior. First, both the theoretical and the experimental results have the same trend in that the activation energy decreases with increasing Te concentrations, as we expected. Second, for high Te concentrations (greater than 10^{19} cm^{-3}), the activation energy is almost equal to zero but the conduction electrons concentrations are much smaller than the Te concentrations. On a quantitative basis there is still a discrepancy between the calculated and measured number of electrons cm^{-3}. The origin of this discrepancy is not known at present.

V. CONCLUSION

For high dose Te implanted Si samples, the number of electrons/cm^2 are found to be much less than the implanted number of Te/cm^2 while the activation energy was approximately equal to zero. By use of layer removal technique in combination with Hall effect and resistivity measurements, we

were able to investigate the electrical properties of Te implanted Si samples in more detail. The effect of the residual radiation damage has been investigated through the simulation of radiation damage by Si ion pre-damage in phosphorus implanted samples. The negligible influence of the residual radiation damage on the electrical properties of phosphorus implanted samples, with or without Si ion pre-damage, led us to assume that the residual radiation damage did not substantially reduce the electron concentrations of the Te implanted Si samples. Quenching of the Te implanted samples after a 1000°C anneal has been found to give little increase of number of conduction electrons/cm^2. Therefore, we do not believe that the formation of inactive substitutional Te clusters is entirely responsible for the much smaller number of conduction electrons/cm^2 as compared to the implanted Te atoms.

Theoretical calculations which included the effects of decrease of activation energy with increasing impurity concentrations gave qualitative agreement with the experiment results. Both the theoretical and experimental results indicated that the activation energy decreases approximately to zero for Te concentration higher than 10^{19} cm^{-3}. Further, not all the Te are ionized even though the activation energy is almost zero. This is understandable from our model of the variation of activation energy with impurity concentrations. In addition to the strictly downward shifting of the conduction band edge, the broadening of impurity states and the smearing of conduction band edge also contribute to the decrease of activation energy with increasing impurity concentrations. Even though the activation energy is almost zero, the Te atoms are not necessarily all ionized.

APPENDIX

Dealing with the variation of activation energy with impurity concentrations, we included three effects in our model. These three effects are (i) the lowering of conduction band edge due to attraction between conduction electrons and ionized donirs, (ii) the broadening of donor level due to donor electron wavefunction overlapping and (iii) the smearing of conduction band edge and the spreading of donor states due to potential fluctuation.

To obtain the lowering of conduction band edge, we proceeded as follows. Due to the overlapping of ionized donor potentials, the average barrier height against electron conduction has been reduced by an amount of ΔE_1,

$$\Delta E_1 = \frac{2q^2 e^{\frac{d}{2\lambda}}}{4\pi\epsilon\epsilon_o(d/2)} - \frac{q^2 e^{-d/\lambda}}{4\pi\epsilon\epsilon_o d} \quad , \qquad \text{(A-1)}$$

where q is electronic charge, $\epsilon = 11.8$ is Si dielectric constant, d is the average distance between ionized donors and λ is the screening length. The average ionized donor a distance d is given by

$$d = (N_D^+)^{-1/3} \quad , \qquad \text{(A-2)}$$

where N_D^+ is the ionized donor concentration. The screening length λ can be expressed in terms of electronic screening through λ_e and ionized impurity screening length λ_i by

$$\lambda = (\lambda_e^{-2} + \lambda_i^{-2})^{-1/2} \quad , \qquad \text{(A-3)}$$

with

$$\lambda_e = \left(\frac{\varepsilon\varepsilon_o K_B T}{q^2 n} \right)^{1/2} \quad \text{for non-degenerate case} \quad , \qquad \text{(A-4)}$$

and

$$\lambda_i = \left[\frac{\varepsilon\varepsilon_o K_B T/q^2}{(n+N_Z)(1 - \frac{n+N_A}{N_D})} \right]^{1/2} + 0.893 \left[\frac{4\pi}{3} (N_A + N_D) \right]^{-1/3} , \qquad \text{(A-5)}$$

where K_B is Boltzmann constant, T is the absolute temperature, n is the conduction electron concentration, N_D and N_A are donor and acceptor concentrations respectively. Due to electronic tunneling, the bottom of conduction band locates below the top of the barrier. Consequently, the total lowering of conduction band edge is equal to

$$\Delta E_c = \Delta E_1 + \Delta E_2 \qquad , \qquad \text{(A-6)}$$

where ΔE_1 is given by Eq. (A-1) and ΔE_2, due to electron tunneling effect, is approximately equal to

$$\Delta E_2 = \frac{2\hbar^2}{m^* d^2} \qquad , \qquad \text{(A-7)}$$

where $m^* = 0.33\ m$ is Si effective mass and d is given by Eq. (A-2).

The average broadening of donor energy level, B, has been found to be

$$B = 2 \int J(R) \cdot 4\pi N_D R^2 \, \text{Exp}(-\tfrac{4\pi}{3} N_D R^3) \, dR \qquad , \qquad \text{(A-8)}$$

where J(R) is the energy transfer integral and is given by

$$J(R) = \frac{Z_{eff}\, q^2}{4\pi\varepsilon\varepsilon_o}(1 + \xi R)e^{-\xi R} \quad , \qquad \text{(A-9)}$$

where Z_{eff} is the effective charge of the donor nucleus and $1/\xi$ is the average radius of donor electron wavefunction. Z_{eff} and ξ have different values for different impurities in Si. For impurities such as P, As or Sb in Si, the hydrogen model is appropriate and thus we have

$$Z_{eff} = 1 \quad , \qquad \text{(A-10)}$$

and

$$\xi = \frac{1}{a_H}\sqrt{\frac{E_D}{E_o}} \quad , \qquad \text{(A-11)}$$

where $a_H \equiv \frac{4\pi\varepsilon\varepsilon_o\hbar^2}{m^* q^2}$ is effective Bohr radius, $E_o = -\frac{q^2}{8\pi\varepsilon\varepsilon_o a_H}$ is the ground state energy from effective mass theory[19] and $(-E_D)$ is the donor ionization energy at low donor concentration case. For impurities such as S or Te in Si, they have two more valence electrons and thus helium model seems to be appropriate.[18] Using helium model, we treated Z_{eff} as parameter such that

$$E_D = E_o\left[Z_{eff}^2 - \frac{5}{4}Z_{eff} + \frac{25}{128}\right] \quad , \qquad \text{(A-12)}$$

i.e.

$$Z_{eff} = \frac{5}{8} + \sqrt{\frac{25}{128} + \frac{E_D}{E_o}} \quad , \qquad \text{(A-13)}$$

and we have

$$\xi = \frac{Z_{eff} - \frac{5}{16}}{a_H} \quad . \qquad \text{(A-14)}$$

Assuming constant density-of-states over the band width B, we have the donor level density-of-states,

$$\rho_o(E) = \begin{cases} N_D/B & -\frac{B}{2} \leq E \leq \frac{B}{2} \\ 0 & \text{otherwise} \end{cases} \quad . \qquad \text{(A-15)}$$

Due to the potential fluctuation, the conduction band and donor level density-of-states have been modified. The work of Kane[20] and Morgan[21] indicated that the potential fluctuation can be approximated by Gaussian distribution with the standard deviation given by

$$\sigma = \left[\frac{(N_D^+ + N_A) q^4}{8\pi \varepsilon^2 \varepsilon_o^2} \lambda \right]^{1/2} \quad , \qquad \text{(A-16)}$$

where λ is the screening length, given by (A-3). Thus, the potential fluctuation is given by

$$p(v) = \frac{1}{\sqrt{2\pi}\,\sigma} e^{-\frac{v^2}{2\sigma^2}} \quad . \qquad \text{(A-17)}$$

The conduction electron mobility is a function of energy in the conduction band tail. For simplicity, we assume that the mobility is constant for electrons with potential energy $\geq -2\sigma$ and mobility is zero for potential energy $< -2\sigma$. The electron with zero mobility would not contribute to current conduction. Therefore, the conduction band density-of-states is given by

$$N_c(E) = \begin{cases} \dfrac{6\sqrt{2}\,(m^*)^{3/2}}{\pi^2 \hbar^3} \displaystyle\int_{-\infty}^{E} (E-V)^{1/2}\, p(v)dv & E \geq -2\sigma \\ 0 & E < -2\sigma \end{cases} \qquad \text{(A-18)}$$

The donor level density-of-states $\rho_i(E)$ should include both the fluctuation induced broadening and the broadening due to the energy transfer integral. These two effects can be combined by averaging $\rho_o(E)$ given in (A-15) over the value of the local potential. That is

$$\rho_i(E) = \int_{-\infty}^{\infty} \rho_o(E-v)\, p(v)dv \quad , \qquad \text{(A-19)}$$

where $p(v)$ is given by (A-17).

REFERENCES

1. J.W. Mayer, L. Eriksson and J.A. Davies, Ion Implantation in Semiconductors, Academic Press, New York (1970).
2. J. Gyulai, O. Meyer, R.D. Pashley and J.W. Mayer. Rad. Effects 7, 17 (1971).
3. S.T. Picraux, N.G.E. Johansson and J.W. Mayer, Semiconductor Silicon, Electrochem. Soc., Inc., New York, 422 (1969)
4. S. Fischler, Metallurgy of Advanced Electronic Materials, Interscience 19, New York (1963).
5. R.D. Pashley, Ph.D. thesis, California Institute of Technology (1973).
6. N.G.E. Johansson, J.W. Mayer and O.J. Marsh, Solid State Elec. 13, 317 (1970).
7. E.H. Putley, The Hall Effect and Semiconductor Physics, Dover Publ., New York (1960).
8. R. Baron, G.A. Shifrin, O.J. Marsh and J.W. Mayer, J. Appl. Phys. 40, 3702 (1969).
9. R.L. Petzitz, Phys. Rev. 110, 1254 (1958).
10. R.D. Pashley, Rad. Effects 11, 1 (1971).
11. R.O. Schwenker, E.S. Pan and R.F. Lever, J. Appl. Phys. 42, 3195 (1971).
12. T. F. Lee and T. C. McGill, to be published.

13. W.J. Johnson and F.J. Gibbons, Projected Range Statistics in Semiconductors, Stanford University Bookstore (1969).

14. L.J. van der Pauw, Phillips Res. Rep. 13, 1 (1958).

15. N.G.E. Johansson and J.W. Mayer, Solid State Elec. 13, 123 (1970).

16. V.I. Fistul, Heavily Doped Semiconductors, Plenum Press, New York (1969).

17. G.L. Pearson and J. Bardeen, Phys. Rev. 75, 865 (1949).

18. A.G. Milnes, Deep Level Impurities in Semiconductors, Wiley-Interscience, New York (1973).

19. W. Kohn, Solid State Physics, Vol. 5 (Academic Press, New York, 1957).

20. E. O. Kane, Phys. Rev. 131, 79 (1963).

21. T. N. Morgan, Phys. Rev. 139, A343 (1965).

SUGGESTION FOR FUTURE WORK:

It has been shown that the EHT can produce silicon band structure with band gap 1.15 eV and with the minimum of conduction band occurring along the $\langle 100 \rangle$ direction; both are in agreement with the accepted silicon band structures. We can apply the same EHT to amorphous silicon to obtain the density-of-states. It is interesting to compare the results obtained by using the EHT with those obtained by using some other methods. Furthermore, the EHT combined with periodic large unit cell has been shown to give good qualitative results for divacancy, a deep level, in silicon. We can extended this method to more complicated systems, such as deep impurities in silicon, and study their properties.

In the theory of variation of activation energies with impurity concentrations, we have assumed that the electron mobility is either a finite constant or zero for electrons in the conduction band tail. However, the electron mobility should be a function of energy. Therefore, we can improve the theory by including the mobility variation in the band tail. This may bring a better agreement between the theory and experiment. Furthermore, the Hall effect and resistivity measurements were performed from room temperature down to 100 K. To provide a check for the theory and to investigate the electrical properties at lower temperatures, it will be important to do Hall effect and resistivity measurements on Te implanted Si samples down to liquid helium temperature.